

The physics of ghost imaging

Yanhua Shih
Department of Physics
University of Maryland, Baltimore County,
Baltimore, MD 21250

Abstract: One of the most surprising consequences of quantum mechanics is the nonlocal behavior of a multi-particle system. Although questions regarding fundamental issues of quantum theory still exist, nonclassical surprises have started to play important roles in practical applications. Ghost imaging is one of these exciting areas. Two types of ghost imaging have been experimentally demonstrated since 1995. Type-one ghost imaging uses entangled photon pairs and type-two ghost imaging uses chaotic light. The unique point-to-point image-forming correlation between the object and image planes in ghost imaging is the result of a constructive-destructive interference which involves the nonlocal superposition of two-photon amplitudes, a nonclassical entity corresponding to different yet indistinguishable alternative ways of triggering a joint-detection event. This article is aimed at exploring and analyzing the quantum nature of ghost imaging. It is true that classical challenges have never stopped. Quantum? Classical? A hot debate is currently focused on ghost imaging. This article defends the quantum mechanical point of view.

1 Introduction

The concept of optical imaging is well defined in classical optics. Figure 1 schematically illustrates a standard imaging setup.

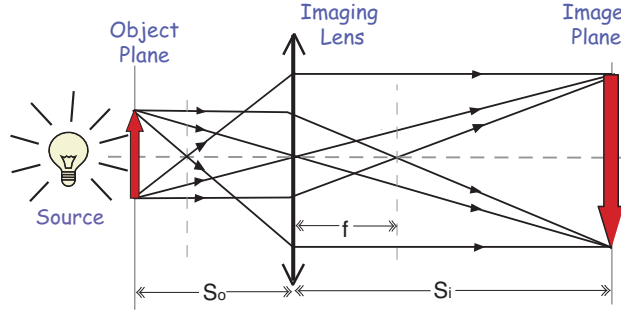


Figure 1: Optical imaging: a lens produces an *image* of an object in the plane defined by the Gaussian thin-lens equation $1/s_i + 1/s_o = 1/f$. Image formation is based on the existence of a point-to-point relationship between the object plane and the image plane.

In this setup an object is illuminated by a radiation source, an imaging lens is used to focus the scattered and reflected light from the object onto an image plane which is defined by the “Gaussian thin lens equation”

$$\frac{1}{s_i} + \frac{1}{s_o} = \frac{1}{f}, \quad (1)$$

where s_o is the distance between the object and the imaging lens, s_i the distance between the imaging lens and the image plane, and f the focal length of the imaging lens. Basically this equation defines a point-to-point relationship between the object plane and the image plane: any radiation starting from a point on the object plane will impinge at a unique point on the image plane. It is not difficult to see from Fig. 1 that the point-to-point relationship is the result of *constructive-destructive interference*. The radiation fields coming from a point on

the object plane will experience equal distance propagation to superpose constructively at one unique point on the image plane, and experience unequal distance propagation to superpose destructively at all other points on the image plane. The use of the imaging lens makes this constructive-destructive interference possible.

A perfect point-to-point image-forming relationship between the object and image planes produces a perfect image. The observed image is a reproduction, either magnified or demagnified, of the illuminated object, mathematically corresponding to a convolution between the object distribution function $f(\vec{\rho}_o)$ and a δ -function which characterizes the perfect point-to-point relationship between the object and image planes:

$$F(\vec{\rho}_i) = \int_{obj} d\vec{\rho}_o f(\vec{\rho}_o) \delta(\vec{\rho}_o + \frac{\vec{\rho}_i}{m}) \quad (2)$$

where $\vec{\rho}_o$ and $\vec{\rho}_i$ are 2-D vectors of the transverse coordinate in the object and image planes, respectively, and $m = s_i/s_o$ is the magnification factor.

In reality, limited by the finite size of the imaging system, we may never have a perfect point-to-point correspondence. The realistic constructive-destructive interference turns the point-to-point correspondence into a point-to-“spot” relationship. The δ -function in the convolution of Eq. (2) will be replaced by a point-spread function:

$$F(\vec{\rho}_i) = \int_{obj} d\vec{\rho}_o f(\vec{\rho}_o) \text{somb}[\frac{R}{s_o} \frac{\omega}{c} |\vec{\rho}_o + \frac{\vec{\rho}_i}{m}|] \quad (3)$$

where the sombrero-like function, or the Airy disk, is defined as

$$\text{somb}(x) = \frac{2J_1(x)}{x},$$

and $J_1(x)$ is the first-order Bessel function, and R the radius of the imaging lens, and R/s_o is known as the numerical aperture of an imaging system. The finite size of the spot, which is defined by the point-spread function or the Airy disk, determines the spatial resolution of the imaging setup. It is clear from Eq. (3) that a larger imaging lens and shorter wavelength will result in a narrower point-spread function, and thus a higher spatial resolution of the image.

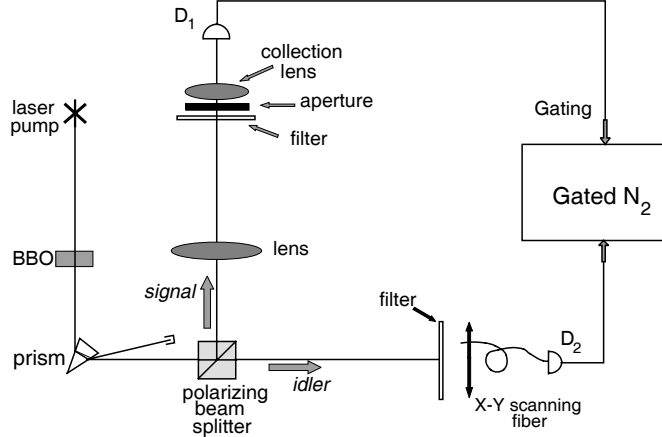


Figure 2: Schematic set-up of the first “ghost” image experiment.

Ghost imaging, in certain aspects, has the same basic feature of classical imaging, such as the unique point-to-point image-forming relationship between the object plane and the image

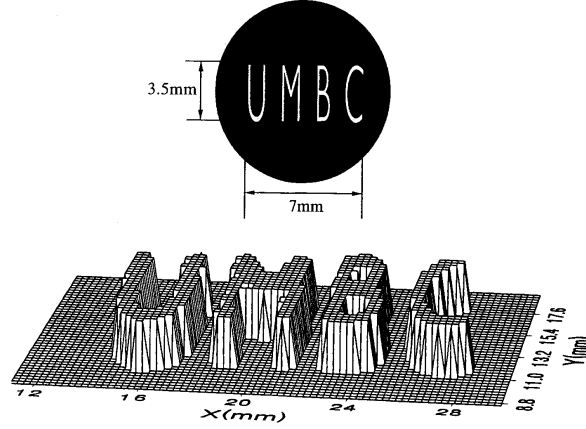


Figure 3: Upper: A reproduction of the actual aperture “UMBC ” placed in the signal beam. Lower: The image of “UMBC”: coincidence counts as a function of the fiber tip’s transverse coordinates in the image plane. The step size is 0.25mm. The image shown is a “slice” at the half maximum value.

plane. Different from classical imaging, the radiation stopped on the imaging plane does not “come” from the object plane. The point-to-point correlation is determined by the nonlocal behavior of a pair of photons: neither photon-one nor photon-two “knows” where to arrive. However, if one of them is observed at a point on the object plane, its twin must arrive at a unique corresponding point on the image plane.

The first ghost imaging experiment was demonstrated by Pittman *et al.* in 1995 [1] [2]. The schematic setup of the experiment is shown in Fig. 2. A continuous wave (CW) laser is used to pump a nonlinear crystal to produce an entangled pair of orthogonally polarized signal (e-ray of the crystal) and idler (o-ray of the crystal) photons in the nonlinear optical process of spontaneous parametric down-conversion (SPDC). The pair emerges from the crystal collinearly with $\omega_s \cong \omega_i \cong \omega_p/2$ (degenerate SPDC). The pump is then separated from the signal-idler pair by a dispersion prism, and the signal and idler are sent in different directions by a polarization beam splitting Thompson prism. The signal photon passes through a convex lens of 400mm focal length and illuminates a chosen aperture (mask). As an example, one of the demonstrations used the letters “UMBC” for the object mask. Behind the aperture is the “bucket” detector package D_1 , which is made by an avalanche photodiode placed at the focus of a short focal length collection lens. During the experiment D_1 is kept in a fixed position. The idler photon is captured by detector package D_2 , which consists of an optical fiber coupled to another avalanche photodiode. The input tip of the fiber is scanned in the transverse plane by two step motors (along orthogonal directions). The output pulses of both detectors, which operate in the photon counting mode, are sent to a coincidence counting circuit for the joint-detection of the signal-idler photon pair. Whenever the following two experimental conditions are satisfactory: (1) D_1 and D_2 always measure a pair; (2) the distances s_o , which is the optical distance between the aperture to the lens, s_i , which is the optical distance from the imaging lens going backward along the signal photon path to the two-photon source of SPDC then going forward along the idler photon path to the fiber tip, and the focal length of the imaging lens f satisfy the Gaussian thin lens equation of Eq. (1), surprisingly, a ghost image of the chosen aperture is observed in coincidences during the scanning of the fiber tip.

Figure 3 reports a typical measured ghost image. It is interesting to note that while the size of the “UMBC” aperture inserted in the signal path is only about 3.5mm×7mm, the observed image measures 7mm×14mm. The image is therefore magnified by a factor of 2 which equals the expected magnification $m = s_i/s_o$. In this measurement $s_o = 600\text{mm}$ and $s_i = 1200\text{mm}$.

When D_2 was scanned on transverse planes other than the ghost image plane the images blurred out.

The experiment was immediately given the name “ghost imaging” due to its nonlocal feature. The experimental demonstration of ghost imaging [1] and ghost interference [3] together stimulated the foundation of quantum imaging in terms of geometrical and physical optics. The 1995 ghost imaging experiment, which took advantage of an entangled photon pair and the Einstein-Poldolsky-Rosen (EPR) two-particle correlation [4], is referred to as type-one ghost imaging.

Type-two ghost imaging uses chaotic radiation sources. Different from type-one, the point-to-point image-forming correlation between the object and image planes is only partial with at least 50% constant background. The first near-field lensless ghost imaging experiment was

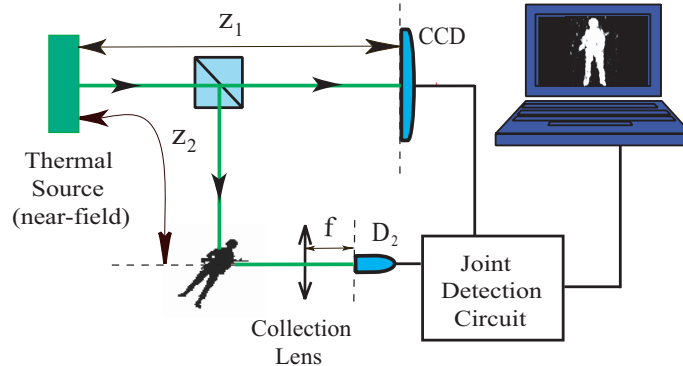


Figure 4: Near-field lensless ghost imaging of chaotic light demonstrated by Meyers *et al.*. D_2 is a point-like photon counting detector that is used to collect and count all randomly scattered and reflected photons from the object. The joint-detection between D_2 and the CCD array is realized by a photon-counting-coincidence circuit. D_2 is fixed in space on the focal plane of a “collection” lens. A ghost image of the object is captured by the gated CCD, when taking $z_1 = z_2$. The images “blurred out” when z_1 is moved away from $z_1 = z_2$.

demonstrated by Scarcelli *et al* in the years of 2005 to 2006 [5][6][7]. Figure 4 is an improved setup of the near-field lensless ghost imaging experiment by Meyers *et al.* [8]. The thermal radiation of a chaotic source, which has a fairly large size in the transverse dimension, is split into two by a 50% – 50% beamsplitter. One of the beams illuminates a toy soldier as shown in Fig. 4. The scattered and reflected photons from the soldier (object) are collected and counted by a “bucket” detector D_2 . In the other beam a high resolution CCD array, operating at single-photon’s level, is placed toward the radiation source for joint-detection with the “bucket” detector D_2 . Surprisingly, a ghost image of the toy soldier is captured by the gated CCD when $z_1 = z_2$.

Although the point-to-point correlation between the object and image planes is only partial it is still a legitimate question to ask: where does it come from? This article is aimed at answering this fundamentally important question. We have concluded that the unique point-to-point correspondence between the object and image planes in ghost imaging is the result of a *constructive-destructive interference* which involves the nonlocal superposition of two-photon amplitudes, a nonclassical entity corresponding to different yet indistinguishable alternative ways of triggering a joint-detection event [9]. This conclusion is valid for both type-one and type-two ghost imaging. To make this point clear we will analyze the physics of ghost imaging in four steps. (1) Review classical imaging as the result of constructive-destructive interference among electromagnetic waves; (2) analyze type-one ghost imaging in terms of constructive-destructive interference between the two-photon amplitudes of an entangled photon-pair; (3)

analyze type-two ghost imaging in terms of two-photon interference between chaotic sub-sources; and (4) discuss the physics of the phenomenon: whether it is a quantum interference effect or a trivial classical intensity fluctuation correlation.

It is interesting to see that the quantum mechanical concept of *two-photon interference* is applicable to “classical” light. To some quantum opticians, perhaps, it is not just interesting but unacceptable. Classical challenges have been attempted by Bennink *et al.* [10], by Gatti *et al.* [11], Wang *et al.* [12], Zhu *et al.* [13], and by Erkmen *et al.* [14]. In fact, this is not the first time in the history of physics we apply quantum mechanical concept to classical light. One should not forget how did Planck apply a quantum mechanical concept to solve the blackbody radiation mystery. The radiation Planck dealt with was classical thermal field. Although the concept of “two-photon superposition” comes from the study of entangled states [9], it is not restricted to entangled systems. The concept is generally true and applicable to any radiation, including classical thermal light.

The observation of the point-to-point partial correlation of thermal radiation is not a new discovery. The first set of intensity-intensity correlation of thermal light was demonstrated by Hanbury Brown and Twiss (HBT) in 1956 [15]. It is true that the HBT phenomenon was successfully interpreted as the classical statistical correlation of intensity fluctuations. It is then reasonable to ask: Is thermal light ghost imaging a simple classical effect similar to that of HBT? Is it possible that ghost imaging itself, including the type-one ghost imaging of 1995, is merely a simple classical effect of intensity fluctuation correlation? Is thermal light ghost imaging “classical” or “quantum”? Is ghost imaging, in general, “classical” or “quantum”? Quantum? Classical? A hot debate is currently focused on the ghost imaging phenomenon [14]. This article defends the quantum mechanical side of the debate.

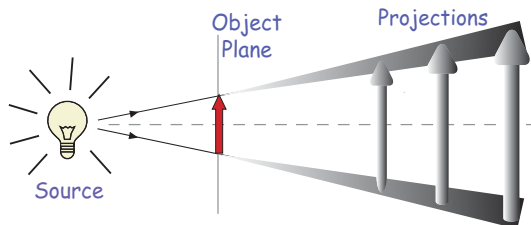


Figure 5: Projection: a light source illuminates an object and no image forming system is present, no image plane is defined, and only projections, or shadows, of the object can be observed.

Before getting into the debate between “quantum” and “classical”, it should be emphasized that one must not confuse a trivial “projection” with an image. Similar to an x-ray photograph, projection makes a shadow of an object, instead of an image of the object. Figure 5 illustrates a projection shadow. It is clear shown that the object-shadow correspondence is essentially defined by the propagation direction of the light rays, and there is no unique imaging plane. The shadow can be found in any plane behind the object. A projection shadow is the result of the simple “blocked-unblocked” effect of light, which is physically different from an imaged image, both from a fundamental and from a practical viewpoint. Our analysis will concentrate on ghost imaging but not on ghost shadow projection.

2 Classical Imaging

We now review classical imaging by starting with a simple question: how does the radiation field propagate from the object plane to the image plane? In classical optics such propagation is usually described by an optical transfer function $h(\mathbf{r} - \mathbf{r}_0, t - t_0)$. We prefer to work with

the single-mode propagator, namely the Green's function, $g(\mathbf{k}, \mathbf{r} - \mathbf{r}_0, t - t_0)$ [18][19], which propagates each mode from space-time point (\mathbf{r}_0, t_0) to space-time point (\mathbf{r}, t) . We will treat the field $E(\mathbf{r}, t)$ as a superposition of these modes. A detailed discussion about $g(\mathbf{k}, \mathbf{r} - \mathbf{r}_0, t - t_0)$ is given in Appendix A. It is convenient to write the field $E(\mathbf{r}, t)$ as a superposition of its longitudinal and transverse modes under the Fresnel paraxial approximation,

$$E(\vec{\rho}, z, t) = \int d\omega d\vec{\kappa} \tilde{E}(\vec{\kappa}, \omega) g(\vec{\kappa}, \omega; \vec{\rho}, z) e^{-i\omega t}, \quad (4)$$

where $\tilde{E}(\omega, \vec{\kappa})$ is the complex amplitude for the mode of frequency ω and transverse wave-vector $\vec{\kappa}$. In Eq. (4) we have taken $z_0 = 0$ and $t_0 = 0$ at the object plane as usual. To simplify the notation, we have assumed one polarization.

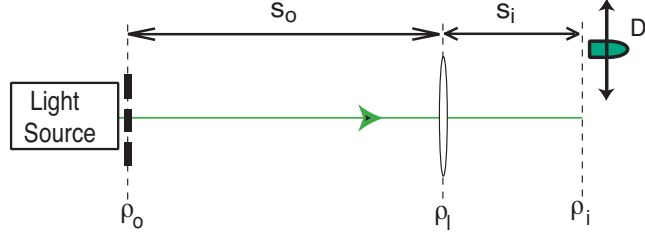


Figure 6: Typical imaging setup. A lens of finite size is used to produce a magnified or demagnified image of an object with limited spatial resolution.

Based on the experimental setup of Fig. 6 and following Appendix A, $g(\vec{\kappa}, \omega; \vec{\rho}, z)$ is found to be

$$\begin{aligned} & g(\vec{\kappa}, \omega; \vec{\rho}_i, s_o + s_i) \\ &= \int_{obj} d\vec{\rho}_o \int_{lens} d\vec{\rho}_l \left\{ A(\vec{\rho}_o) e^{i\vec{\kappa} \cdot \vec{\rho}_o} \right\} \left\{ \frac{-i\omega}{2\pi c} \frac{e^{i\frac{\omega}{c}s_o}}{s_o} e^{i\frac{\omega}{2cs_o}|\vec{\rho}_l - \vec{\rho}_o|^2} \right\} \left\{ e^{-i\frac{\omega}{2cs_i}|\vec{\rho}_i|^2} \right\} \\ & \quad \times \left\{ \frac{-i\omega}{2\pi c} \frac{e^{i\frac{\omega}{c}s_i}}{s_i} e^{i\frac{\omega}{2cs_i}|\vec{\rho}_i - \vec{\rho}_l|^2} \right\}, \end{aligned} \quad (5)$$

where $\vec{\rho}_o$, $\vec{\rho}_l$, and $\vec{\rho}_i$ are two-dimensional vectors defined, respectively, on the object, lens, and image planes. The first curly bracket includes the aperture function $A(\vec{\rho}_o)$ of the object and the phase factor $e^{i\vec{\kappa} \cdot \vec{\rho}_o}$ contributed at the object plane by each transverse mode $\vec{\kappa}$. The terms in the second and fourth curly brackets describe free-space Fresnel propagation-diffraction from the source/object plane to the imaging lens, and from the imaging lens to the detection plane, respectively. The Fresnel propagator includes a spherical wave function $e^{i\frac{\omega}{c}(z_j - z_k)}/(z_j - z_k)$ and a Fresnel phase factor $e^{i\omega|\vec{\rho}_j - \vec{\rho}_k|^2/2c(z_j - z_k)}$. The third curly bracket adds the phase factor introduced by the imaging lens.

We now rewrite Eq. (5) into the following form

$$\begin{aligned} & g(\vec{\kappa}, \omega; \vec{\rho}_i, z = s_o + s_i) \\ &= \frac{-\omega^2}{(2\pi c)^2 s_o s_i} e^{i\frac{\omega}{c}(s_o + s_i)} e^{i\frac{\omega}{2cs_i}|\vec{\rho}_i|^2} \int_{obj} d\vec{\rho}_o A(\vec{\rho}_o) e^{i\frac{\omega}{2cs_o}|\vec{\rho}_o|^2} e^{i\vec{\kappa} \cdot \vec{\rho}_o} \\ & \quad \times \int_{lens} d\vec{\rho}_l e^{i\frac{\omega}{2c}[\frac{1}{s_o} + \frac{1}{s_i} - \frac{1}{f}]|\vec{\rho}_l|^2} e^{-i\frac{\omega}{c}(\frac{\vec{\rho}_o}{s_o} + \frac{\vec{\rho}_i}{s_i}) \cdot \vec{\rho}_l}. \end{aligned} \quad (6)$$

The image plane is defined by the Gaussian thin-lens equation of Eq. (1). Hence, the second integral in Eq. (6) reduces to, for a finite sized lens of radius R , the so-called point-spread function, or the Airy disk, of the imaging system:

$$\int_{lens} d\vec{\rho}_l e^{-i\frac{\omega}{c}(\frac{\vec{\rho}_o}{s_o} + \frac{\vec{\rho}_i}{s_i}) \cdot \vec{\rho}_l} = \frac{2J_1(x)}{x} = \text{somb}(x), \quad (7)$$

where the sombrero-like function $somb(x) = 2J_1(x)/x$ with argument $x = [\frac{R}{s_o} \frac{\omega}{c} |\vec{\rho}_o + \rho_i/m|]$ has been defined in Eq. (3).

Substituting Eqs. (6) and (7) into Eq. (4) enables one to obtain the classical self-correlation function of the field, or, equivalently, the intensity on the image plane

$$I(\vec{\rho}_i, z_i, t_i) = \langle E^*(\vec{\rho}_i, z_i, t_i) E(\vec{\rho}_i, z_i, t_i) \rangle, \quad (8)$$

where $\langle \dots \rangle$ denotes an ensemble average. To simplify the mathematics, monochromatic light is assumed as usual.

Case (I): *Incoherent imaging*. The ensemble average of $\langle \tilde{E}^*(\vec{\kappa}, \omega) \tilde{E}(\vec{\kappa}', \omega) \rangle$ yields zeros except when $\vec{\kappa} = \vec{\kappa}'$. The image is thus

$$I(\vec{\rho}_i) \propto \int d\vec{\rho}_o |A(\vec{\rho}_o)|^2 |somb[\frac{R}{s_o} \frac{\omega}{c} |\vec{\rho}_o + \frac{\vec{\rho}_i}{m}|]|^2. \quad (9)$$

An incoherent image, magnified by a factor of m , is thus given by the convolution between the modulus square of the object aperture function and the point-spread function. The spatial resolution of the image is determined by the finite width of the $|somb|^2$ -function.

Case (II): *Coherent imaging*. The coherent superposition of the $\vec{\kappa}$ modes in both $E^*(\vec{\rho}_i, \tau)$ and $E(\vec{\rho}_i, \tau)$ results in a wavepacket. The image, or the intensity distribution on the image plane, is

$$I(\vec{\rho}_i) \propto \left| \int_{obj} d\vec{\rho}_o A(\vec{\rho}_o) e^{i\frac{\omega}{2cs_o} |\vec{\rho}_o|^2} somb[\frac{R}{s_o} \frac{\omega}{c} |\vec{\rho}_o + \frac{\vec{\rho}_i}{m}|] \right|^2. \quad (10)$$

A coherent image, magnified by a factor of m , is thus given by the modulus square of the convolution between the object aperture function (multiplied by a Fresnel phase factor) and the point-spread function.

For $s_i < s_o$ and $s_o > f$, both Eqs. (9) and (10) describe a real demagnified inverted image. In both cases, a narrower *somb*-function yields a higher spatial resolution. Therefore the use of a larger imaging lens and shorter wavelengths will improve the spatial resolution of an imaging system.

3 Entangled two-photon state and type-one ghost imaging

In this section we turn to quantum imaging by replacing the classical light source with an entangled two-photon state such as the signal-idler photon pair of SPDC [20][9]. The nearly collinear signal-idler system generated by SPDC can be described, in the ideal case, by the following non-factorizable two-photon state [9]:

$$|\Psi\rangle = \Psi_0 \int d\vec{\kappa}_s d\vec{\kappa}_i \delta(\vec{\kappa}_s + \vec{\kappa}_i) \int d\omega_s d\omega_i \delta(\omega_s + \omega_i - \omega_p) a^\dagger(\vec{\kappa}_s, \omega_s) a^\dagger(\vec{\kappa}_i, \omega_i) |0\rangle, \quad (11)$$

where $\omega_j, \vec{\kappa}_j$ ($j = s, i, p$), are the frequency and transverse wavevector of the signal, idler, and pump, respectively. For simplicity a CW single mode pump with $\vec{\kappa}_p = 0$ is assumed. Let us imagine a measurement in which two point-like photon counting detectors (D_1 and D_2) are placed at the output plane of a SPDC source. The joint-detection probability between D_1 and D_2 located at $(\vec{\rho}_s, z_s)$ and $(\vec{\rho}_i, z_i)$, respectively, is calculated from the Glauber theory of photodetection [24]:

$$\begin{aligned} & G^{(2)}(\vec{\rho}_s, z_s, t_s; \vec{\rho}_i, z_i, t_i) \\ &= \langle \Psi | E_s^{(-)}(\vec{\rho}_s, z_s, t_s) E_i^{(-)}(\vec{\rho}_i, z_i, t_i) E_i^{(+)}(\vec{\rho}_i, z_i, t_i) E_s^{(+)}(\vec{\rho}_s, z_s, t_s) | \Psi \rangle \\ &= |\langle 0 | E_i^{(+)}(\vec{\rho}_i, z_i, t_i) E_s^{(+)}(\vec{\rho}_s, z_s, t_s) | \Psi \rangle|^2 \\ &\equiv |\Psi(\vec{\rho}_s, z_s, t_s; \vec{\rho}_i, z_i, t_i)|^2, \end{aligned} \quad (12)$$

where $\Psi(\vec{\rho}_s, z_s, t_s; \vec{\rho}_i, z_i, t_i)$ is defined as the effective two-photon wavefunction. Taking $z_s = z_i = 0$, the transverse part of the effective two-photon wavefunction $\Psi(\vec{\rho}_s, \vec{\rho}_i)$ is calculated to be:

$$\Psi(\vec{\rho}_s, \vec{\rho}_i) \simeq \Psi_0 \delta(\vec{\rho}_s - \vec{\rho}_i). \quad (13)$$

Equations (11) and (13) suggest that the entangled signal-idler photon pair is characterized by the EPR correlation [4] in transverse momentum and transverse position; hence, similar to the original EPR state, we have [21]:

$$\begin{aligned} \Delta(\vec{\kappa}_s + \vec{\kappa}_i) = 0 \quad \& \quad \Delta(\vec{\rho}_s - \vec{\rho}_i) = 0 \\ \text{with } \Delta\vec{\kappa}_s \sim \infty, \quad \Delta\vec{\kappa}_i \sim \infty, \quad \Delta\vec{\rho}_s \sim \infty, \quad \Delta\vec{\rho}_i \sim \infty. \end{aligned} \quad (14)$$

In EPR's language, the signal photon and the idler photon may come from any point in the output plane of the SPDC. However, if the signal (idler) is found in a certain position, the idler (signal) must be observed in the same position, with certainty (100%). Simultaneously, the signal photon and the idler photon may have any transverse momentum. However, if a certain value and direction of the transverse momentum of the signal (idler) is observed, the transverse momentum of the idler (signal) will be uniquely determined with equal value and opposite direction.

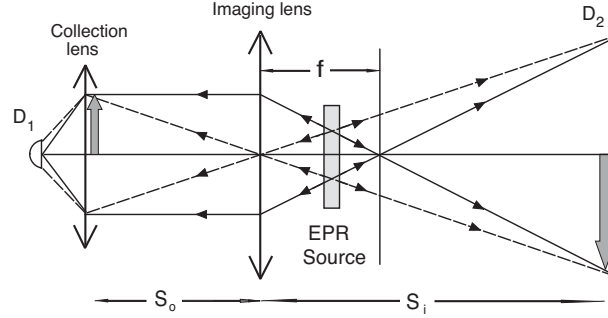


Figure 7: An unfolded schematic of the 1995 ghost imaging experiment, which is helpful for understanding the physics. Since the two-photon “light” propagates along “straight lines”, it is obvious that any point on the object plane corresponds to a unique point on the image plane. Although the placement of the lens, the object, and detector D_2 obeys the Gaussian thin lens equation, it is important to notice that the geometric rays in the figure actually represent the two-photon amplitudes of an entangled photon pair. The point-to-point correspondence is the result of a constructive-destructive superposition of these two-photon amplitudes.

The EPR δ -functions, $\delta(\vec{\rho}_s - \vec{\rho}_i)$ and $\delta(\vec{\kappa}_s + \vec{\kappa}_i)$ in transverse position and momentum, are the key to understanding the ghost imaging experiment of Pittman *et al.* of 1995. $\delta(\vec{\rho}_s - \vec{\rho}_i)$ indicates that the signal-idler pair is always emitted from the same point on the output plane of the biphoton source. Simultaneously, $\delta(\vec{\kappa}_s + \vec{\kappa}_i)$ defines the angular correlation of the pair: the signal-idler pair always exist at roughly equal but opposite angles relative to the pump for degenerate SPDC. This then allows for a simple explanation of the experiment in terms of “usual” geometrical optics in the following manner: we envision the nonlinear crystal as a “hinge point” and “unfold” the schematic of Fig. 2 into the Klyshko picture [2] of Fig. 7. The signal-idler two-photon amplitudes can then be represented by straight lines (but keep in mind the different propagation directions) and therefore the image is reproduced in coincidences when the aperture, lens, and fiber tip are located according to the Gaussian thin lens equation of Eq. (1). The image is exactly the same as that one would observe on a screen placed at the fiber tip if detector D_1 were replaced by a point-like light source and the nonlinear crystal by a reflecting mirror.

Comparing the “unfolded” schematic of the ghost imaging experiment with that of the classical imaging setup of Fig. 1, it is not difficult to find that any “light point” on the object plane has a unique corresponding “light point” on the image plane. This point-to-point correspondence is the result of the constructive-destructive interference among these biphoton amplitudes that are illustrated as geometrical rays in Fig. 7. Similar to the situation in classical imaging, these biphoton amplitudes which experience equal optical path propagation will superpose constructively at a pair of object-imaging points for a joint-detection event, while these that experience unequal distance propagation will superpose destructively at all other points on the object and image planes. The use of the imaging lens makes this constructive-destructive interference possible. It is this unique point-to-point EPR correlation that makes the “ghost” image of the object-aperture function possible. Despite the completely different physics from classical optics, the remarkable feature is that the relationship between the focal length f of the lens, the aperture’s optical distance s_o , and the image’s optical distance s_i , satisfies the Gaussian thin lens equation of Eq. (1). It is worth to emphasize again that the geometric rays in Fig. 7 represent the two-photon amplitudes of a signal-idler photon pair, and the point-to-point correspondence is the result of the constructive-destructive superposition of these two-photon amplitudes.

Let us examine $G^{(2)}(\vec{\rho}_1, \vec{\rho}_2)$ for the “ghost” imaging experiment, where $\vec{\rho}_1$ and $\vec{\rho}_2$ are the transverse coordinates of the point-like photodetector D_1 and D_2 , on the object and image planes, respectively. We will show that there exists a δ -function-like point-to-point correlation between the object and image planes, $\delta(\vec{\rho}_1 - \vec{\rho}_2/m)$. We will then show how the object function of $A(\vec{\rho}_o)$ is transferred to the image plane as a magnified image $A(\vec{\rho}_2/m)$.

We first calculate the effective two-photon wavefunction $\Psi(\vec{\rho}_1, z_1, t_1; \vec{\rho}_2, z_2, t_2)$, as defined in Eq. (12). By inserting the field operators into $\Psi(\vec{\rho}_1, z_1, t_1; \vec{\rho}_2, z_2, t_2)$, and considering the commutation relations of the field operators, the effective two-photon wavefunction is found to be

$$\begin{aligned} \Psi(\vec{\rho}_1, z_1, t_1; \vec{\rho}_2, z_2, t_2) = & \Psi_0 \int d\vec{\kappa}_s d\vec{\kappa}_i \delta(\vec{\kappa}_s + \vec{\kappa}_i) \int d\omega_s d\omega_i \delta(\omega_s + \omega_i - \omega_p) \\ & \times g(\vec{\kappa}_s, \omega_s; \vec{\rho}_1, z_1) e^{-i\omega_s t_1} g(\vec{\kappa}_i, \omega_i; \vec{\rho}_2, z_2) e^{-i\omega_i t_2}. \end{aligned} \quad (15)$$

Equation (15) indicates a coherent superposition of all the two-photon amplitudes shown in Fig. 7. Next, we follow the unfolded experimental setup shown in Fig. 8 to establish the Green’s functions $g(\vec{\kappa}_s, \omega_s, \vec{\rho}_1, z_1)$ and $g(\vec{\kappa}_i, \omega_i, \vec{\rho}_2, z_2)$. In arm-1 the signal propagates freely over a distance d_1 from the output plane of the source to the imaging lens, passes an object aperture at distance s_o , and then is focused onto photon-counting detector D_1 by a collection lens. We will evaluate $g(\vec{\kappa}_s, \omega_s, \vec{\rho}_1, z_1)$ by propagating the field from the output plane of the biphoton source to the object plane. In arm-2 the idler propagates freely over a distance d_2 from the output plane of the biphoton source to a point-like detector D_2 . $g(\vec{\kappa}_i, \omega_i, \vec{\rho}_2, z_2)$ is thus a free propagator.

(I) Arm-1 (source to object):

The optical transfer function or Green’s function in arm-1, which propagates the field from the source plane to the object plane, is given by:

$$\begin{aligned} g(\vec{\kappa}_s, \omega_s; \vec{\rho}_1, z_1 = d_1 + s_o) = & e^{i\frac{\omega_s}{c} z_1} \int_{lens} d\vec{\rho}_l \int_{source} d\vec{\rho}_s \left\{ \frac{-i\omega_s}{2\pi c d_1} e^{i\vec{\kappa}_s \cdot \vec{\rho}_s} e^{i\frac{\omega_s}{2c d_1} |\vec{\rho}_s - \vec{\rho}_l|^2} \right\} \\ & \times e^{-i\frac{\omega_s}{2c f} |\vec{\rho}_l|^2} \left\{ \frac{-i\omega_s}{2\pi c s_o} e^{i\frac{\omega_s}{2c s_o} |\vec{\rho}_l - \vec{\rho}_1|^2} \right\}, \end{aligned} \quad (16)$$

where $\vec{\rho}_s$ and $\vec{\rho}_l$ are the transverse vectors defined, respectively, on the output plane of the source and on the plane of the imaging lens. The terms in the first and second curly brackets in Eq. (16) describe free space propagation from the output plane of the source to the imaging lens and from the imaging lens to the object plane, respectively. Again, $e^{i\frac{\omega_s}{2c d_1} |\vec{\rho}_s - \vec{\rho}_l|^2}$ and

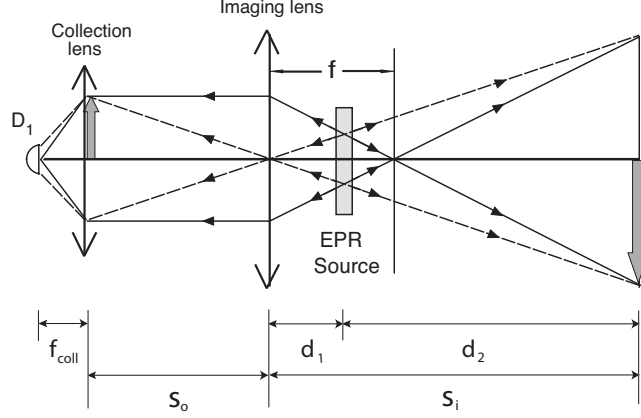


Figure 8: In arm-1 the signal propagates freely over a distance d_1 from the output plane of the source to the imaging lens, passes an object aperture at distance s_o , and then is focused onto photon-counting detector D_1 by a collection lens. In arm-2 the idler propagates freely over a distance d_2 from the output plane of the source to a point-like photon counting detector D_2 .

$e^{i\frac{\omega_s}{2cs_o}|\vec{\rho}_l - \vec{\rho}_1|^2}$ are the Fresnel phases as defined in Appendix A. Here the imaging lens is treated as a thin-lens, and the transformation function of the imaging lens is approximated as a Gaussian, $l(|\vec{\rho}_l|, f) \cong e^{-i\frac{\omega}{2cf}|\vec{\rho}_l|^2}$.

(II) Arm-2 (from source to image):

In arm-2, the idler propagates freely from the source to the plane of D_2 , which is also the plane of the image. The Green's function is

$$g(\vec{\kappa}_i, \omega_i; \vec{\rho}_2, z_2 = d_2) = \frac{-i\omega_i}{2\pi c d_2} e^{i\frac{\omega_i}{c}d_2} \int_{source} d\vec{\rho}'_s e^{i\frac{\omega_i}{2cd_2}|\vec{\rho}'_s - \vec{\rho}_2|^2} e^{i\vec{\kappa}_i \cdot \vec{\rho}'_s} \quad (17)$$

where $\vec{\rho}'_s$ and $\vec{\rho}_2$ are the transverse vectors defined, respectively, on the output plane of the source and the plane of photodetector D_2 .

(III) $\Psi(\vec{\rho}_1, \vec{\rho}_2)$ and $G^{(2)}(\vec{\rho}_1, \vec{\rho}_2)$ (object plane - image plane):

For simplicity, in the following calculation we consider degenerate ($\omega_s = \omega_i = \omega$) and collinear SPDC. The transverse two-photon effective wavefunction $\Psi(\vec{\rho}_1, \vec{\rho}_2)$ is then evaluated by substituting the Green's functions $g(\vec{\kappa}_s, \omega; \vec{\rho}_1, z_1)$ and $g(\vec{\kappa}_i, \omega; \vec{\rho}_2, z_2)$ into Eq. (15),

$$\begin{aligned} \Psi(\vec{\rho}_1, \vec{\rho}_2) &\propto \int d\vec{\kappa}_s d\vec{\kappa}_i \delta(\vec{\kappa}_s + \vec{\kappa}_i) g(\vec{\kappa}_s, \omega; \vec{\rho}_1, z_1) g(\vec{\kappa}_i, \omega; \vec{\rho}_2, z_2) \\ &\propto e^{i\frac{\omega}{c}(s_o + s_i)} \int d\vec{\kappa}_s d\vec{\kappa}_i \delta(\vec{\kappa}_s + \vec{\kappa}_i) \int_{lens} d\vec{\rho}_l \int_{source} d\vec{\rho}_s e^{i\vec{\kappa}_s \cdot \vec{\rho}_s} e^{i\frac{\omega}{2cd_1}|\vec{\rho}_s - \vec{\rho}_l|^2} \\ &\quad \times e^{-i\frac{\omega}{2cf}|\vec{\rho}_l|^2} e^{i\frac{\omega_s}{2cs_o}|\vec{\rho}_l - \vec{\rho}_1|^2} \int_{source} d\vec{\rho}'_s e^{i\vec{\kappa}_i \cdot \vec{\rho}'_s} e^{i\frac{\omega_i}{2cd_2}|\vec{\rho}'_s - \vec{\rho}_2|^2} \end{aligned} \quad (18)$$

where all the proportionality constants have been ignored. After completing the double integral of $d\vec{\kappa}_s$ and $d\vec{\kappa}_i$

$$\int d\vec{\kappa}_s d\vec{\kappa}_i \delta(\vec{\kappa}_s + \vec{\kappa}_i) e^{i\vec{\kappa}_s \cdot \vec{\rho}_s} e^{i\vec{\kappa}_i \cdot \vec{\rho}'_s} \sim \delta(\vec{\rho}_s - \vec{\rho}'_s),$$

Eq. (18) becomes

$$\Psi(\vec{\rho}_1, \vec{\rho}_2) \propto e^{i\frac{\omega}{c}(s_0+s_i)} \int_{lens} d\vec{\rho}_l \int_{source} d\vec{\rho}_s e^{i\frac{\omega}{2cd_2}|\vec{\rho}_2-\vec{\rho}_s|^2} e^{i\frac{\omega}{2cd_1}|\vec{\rho}_s-\vec{\rho}_l|^2} e^{-i\frac{\omega}{2cf}|\vec{\rho}_l|^2} e^{i\frac{\omega}{2cs_o}|\vec{\rho}_l-\vec{\rho}_o|^2}.$$

Next, we complete the integral for $d\vec{\rho}_s$,

$$\Psi(\vec{\rho}_1, \vec{\rho}_2) \propto e^{i\frac{\omega}{c}(s_0+s_i)} \int_{lens} d\vec{\rho}_l e^{i\frac{\omega}{2cs_i}|\vec{\rho}_2-\vec{\rho}_l|^2} e^{-i\frac{\omega}{2cf}|\vec{\rho}_l|^2} e^{i\frac{\omega}{2cs_o}|\vec{\rho}_l-\vec{\rho}_o|^2}, \quad (19)$$

where we have replaced $d_1 + d_2$ with s_i (as depicted in Fig. 8). Although the signal and idler propagate in different directions along two optical arms, interestingly, the Green function in Eq. (19) is equivalent to that of a classical imaging setup, by imagining the fields start propagating from a point $\vec{\rho}_1$ on the object plane to the lens and then stop at point $\vec{\rho}_2$ on the imaging plane. The mathematics is consistent with our previous qualitative analysis of the experiment.

The finite integral on $d\vec{\rho}_l$ yields a point-to-“spot” relationship between the object plane and the image plane that is defined by the Gaussian thin-lens equation

$$\Psi(\vec{\rho}_1, \vec{\rho}_2) \propto \int_{lens} d\vec{\rho}_l e^{i\frac{\omega}{2c}[\frac{1}{s_o}+\frac{1}{s_i}-\frac{1}{f}]|\vec{\rho}_l|^2} e^{-i\frac{\omega}{c}(\frac{\vec{\rho}_1}{s_o}+\frac{\vec{\rho}_2}{s_i})\cdot\vec{\rho}_l} = \text{somb}\left(\frac{R}{s_o} \frac{\omega}{c}|\vec{\rho}_1 + \frac{\vec{\rho}_2}{m}|\right). \quad (20)$$

If the integral is taken to infinity, by imposing the condition of the Gaussian thin-lens equation the transverse two-photon effective wavefunction can be approximated as a δ function

$$\Psi(\vec{\rho}_1, \vec{\rho}_2) \sim \delta(\vec{\rho}_1 + \vec{\rho}_2/m) \sim \delta(\vec{\rho}_o + \vec{\rho}_I/m), \quad (21)$$

where we have replaced $\vec{\rho}_1$ and $\vec{\rho}_2$ with $\vec{\rho}_o$ and $\vec{\rho}_I$, respectively, to emphasize the point-to-point EPR correlation between the object and image planes. To avoid confusion with the “idler” we have used $\vec{\rho}_I$ to label the image plane.

We now include an object-aperture function, a collection lens and a photon counting detector D_1 into the optical transfer function of arm-1 as shown in Fig. 2. The collection-lens- D_1 package can be simply treated as a “bucket” detector. The “bucket” detector integrates the two-photon amplitudes $\Psi(\vec{\rho}_o, \vec{\rho}_2)$, which are modulated by the object aperture function $A(\vec{\rho}_o)$ into a joint photodetection event. This process is equivalent to the following convolution

$$R_{1,2} \propto \int_{object} d\vec{\rho}_o |A(\vec{\rho}_o)|^2 |\Psi(\vec{\rho}_o, \vec{\rho}_2)|^2 \simeq |A(\vec{\rho}_2/m)|^2 = |A(\vec{\rho}_I/m)|^2. \quad (22)$$

Again, D_2 is scanned in the image plane ($\vec{\rho}_2 = \vec{\rho}_I$). A ghost image of the object is thus reproduced on the image plane by means of the joint-detection between the point-like-detector D_2 and the bucket detector D_1 .

The observation of type-one ghost imaging has demonstrated a point-to-point EPR correlation between the object and image planes. This point-to-point correlation is the result of a constructive-destructive superposition between two-photon amplitudes,

$$G^{(2)}(\vec{\rho}_o, \vec{\rho}_I) = \left| \int d\vec{\kappa}_s d\vec{\kappa}_i \delta(\vec{\kappa}_s + \vec{\kappa}_i) g(\vec{\kappa}_s, \vec{\rho}_o) g(\vec{\kappa}_i, \vec{\rho}_I) \right|^2. \quad (23)$$

In this view we consider the ghost imaging experiment of Pittman *et al.* as a realization of the 1935 EPR *gedankenexperiment* [21] [22].

It is necessary to emphasize that one should not confuse a trivial coincidence ghost shadow projection with ghost imaging. A typical ghost shadow experiment was demonstrated by Benink *et al.* in 2002 [10] to challenge the quantum nature of ghost imaging. Figure 9 is a schematic

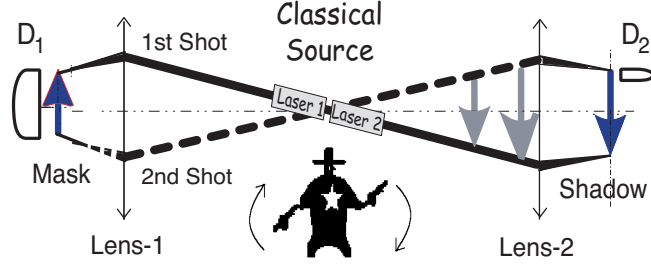


Figure 9: The projection shadow of an object mask is observed in coincidences between D_1 and D_2 by the use of two correlated co-rotating laser beams. The shadow is the result of a trivial “blocked-unblocked” effect of light.

picture of their experiment. Different from ghost imaging, in which the point-to-point image-forming correlation between the object and image planes is the result of a nonlocal two-photon constructive-destructive interference, here the point-to-point correspondence is made artificially by two “classically correlated” co-rotating laser beams “shot by shot”. The laser beams propagated to opposite directions and focused on the object and image planes, respectively. If laser beam-1 is blocked by the object mask there would be no joint-detection between D_1 and D_2 for that “shot”, while if laser beam-1 is unblocked, a coincidence count will be recorded against that angular position of the co-rotating laser beams. A shadow of the object mask is then reconstructed in coincidences. This projection shadow is physically different from an imaged ghost image, both from a fundamental and from a practical viewpoint. In fact, the experiment of Bennink *et al.* is an excellent example to distinguish a trivial classical correlation from quantum entanglement and from nonlocal superposition of a multi-quantum system.

4 Type-two ghost imaging with chaotic radiation

In this section we discuss the physics of thermal light ghost imaging. The near-field lensless ghost imaging with thermal radiation was first demonstrated by Scarcelli *et al.* in the years from 2005 to 2006 [5]. The schematic experimental setup is shown in Fig. 10. A chaotic radiation source, with a narrow temporal bandwidth $\Delta\omega$ and a large spatial frequency bandwidth Δk_x , is divided equally into two by a 50% – 50% beam-splitter. The reflected light propagates and focuses onto a point-like photodetector D_2 after passing through an object mask, which is a simple double-slit in Fig. 10. D_2 is fixed on the focus of a convex lens. It is clear that D_2 cannot “see” any spatial distribution, or the aperture function of the object mask. The transmitted light freely propagates to the plane of x_1 to be detected by the scanning point-like photodetector D_1 . The joint-detection between D_1 and D_2 is realized either by a photon-counting coincidence counter or by a standard HBT type current-current correlator. An equal sized 1-D image of the object mask is then observed in the joint-detection when D_1 is scanned in the plane of $z_1 = z_2$ along the x_1 -axis. The image contrast is observed to be almost 50% in amplitude, which is the maximum achievable visibility we can expect. It is the partial point-to-point correlation between the object plane, $z_1 = z_0$, and the image plane, $z_2 = z_0$, that makes ghost imaging with chaotic light possible.

The partial point-to-point correlation of thermal light is not a new discovery. The first example of second-order correlation of thermal light was demonstrated in 1956 by Hanbury Brown and Twiss (HBT) with two different types of correlations: temporal and spatial [15][16]. The HBT experiment created quite a surprise in the physics community which has evolved into an enduring debate about the classical or quantum nature of the phenomenon [16][17]. Figure 11 is a schematic of the historical HBT experiment which measures the second-order transverse spatial correlation of a far-field monochromatic radiation source of wavelength λ such

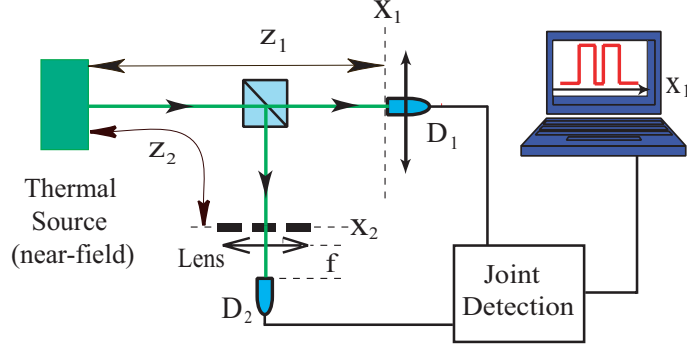


Figure 10: Near-field lensless ghost imaging with chaotic light demonstrated in 2006 by Scarcelli *et al.* D_1 and D_2 are point-like photodetectors. The joint-detection between D_1 and D_2 is realized either by a photon-counting coincidence counter or by a standard HBT type current-current correlator. In this measurement D_2 is fixed in the focus of a convex lens. An image of the 1-D object is observed in the joint-detection between D_1 and D_2 by scanning D_1 in the plane of $z_1 = z_2$ along the x_1 -axis. The image, however, blurred out when $z_1 \neq z_2$.

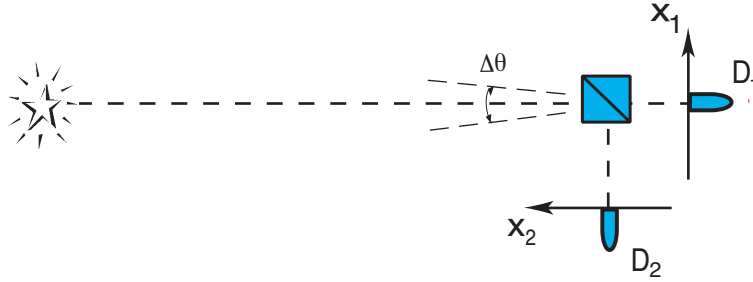


Figure 11: Schematic of the historical Hanbury Brown and Twiss experiment which measures the second-order transverse correlation of a far-field chaotic radiation source.

as a distant star. If we perform the measurement in 1-D by scanning photodetectors D_1 and D_2 along the axes x_1 and x_2 . The second-order transverse spatial correlation function $\Gamma^{(2)}(x_1, x_2)$ is measured to be

$$\Gamma^{(2)}(x_1, x_2) = \langle I_1 I_2 \rangle \sim I_0^2 \left\{ 1 + \text{sinc}^2 \left[\frac{\pi \Delta \theta (x_1 - x_2)}{\lambda} \right] \right\}, \quad (24)$$

where $\Delta \theta$ is the angular size of the star. The far-field HBT correlation of Eq. (24) has been interpreted as the classical statistical correlation of the intensity fluctuations:

$$\langle \Delta I_1 \Delta I_2 \rangle = \langle (I_1 - \bar{I}_1)(I_2 - \bar{I}_2) \rangle = \langle I_1 I_2 \rangle - \bar{I}_1 \bar{I}_2, \quad (25)$$

where \bar{I}_1 and \bar{I}_2 are the mean intensities of the radiation measured by photodetectors D_1 and D_2 , respectively. The second term in Eq. (24), $I_0^2 \text{sinc}^2[\pi \Delta \theta (x_1 - x_2)/\lambda]$, corresponds to the intensity fluctuation correlation $\langle \Delta I_1 \Delta I_2 \rangle$. For short wavelengths this function quickly drops from its maximum to minimum when $x_1 - x_2$ goes from zero to a value such that $\Delta \theta (x_1 - x_2)/\lambda = 1$. Thus we effectively have a “point-to-point” relationship between the x_1 and x_2 axes: for each value of x_1 there exists only one value of x_2 that may have a nonzero intensity fluctuation correlation.

The classical interpretation of the HBT correlation is based on the theory of statistical correlations of intensity fluctuation. In HBT the measurement is taken in the far-field zone

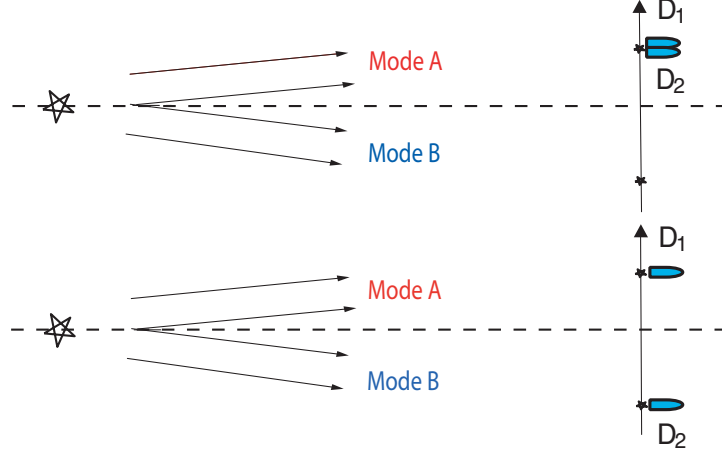


Figure 12: The far-field HBT measurement. Upper: the two photodetectors receive identical modes of the far-field radiation, corresponding to a single point sub-source of the distant star, and thus experience identical intensity fluctuations. The HBT measurement gives a maximum value of $\langle \Delta I_1 \Delta I_2 \rangle$. Lower: the two photodetectors receive different modes of the far-field radiation, corresponding to different point-sub-sources of the distant star. Due to its chaotic nature, different modes of thermal radiation fluctuate independently and randomly. In this case the HBT measurement gives $\langle \Delta I_1 \Delta I_2 \rangle = 0$.

of the radiation source, which is equivalent to the Fourier transform plane. When D_1 (D_2) is scanned in the neighborhood of $x_1 = x_2$, the two detectors measure the same spatial mode of the radiation field, corresponding to the same point-sub-source of the distant star. The measured intensities have the same fluctuations in this case and thus yield a maximum value of $\langle \Delta I_1 \Delta I_2 \rangle$ in the expression $\langle I_1 I_2 \rangle = \bar{I}_1 \bar{I}_2 + \langle \Delta I_1 \Delta I_2 \rangle$. When the two photodetectors move apart with certain a distance, D_1 and D_2 measure different spatial modes of the radiation field, corresponding to different point-sub-sources of the distant star. In this case, due to the chaotic nature of the radiation the measured intensities may have completely different fluctuations. The measurement yields $\langle \Delta I_1 \Delta I_2 \rangle = 0$ and gives $\langle I_1 I_2 \rangle = \bar{I}_1 \bar{I}_2$. Figure 12 illustrates these two different situations. The theory of the statistical correlation of intensity fluctuation has thus provided a phenomenologically reasonable interpretation to the far-field HBT phenomenon.

The above classical theory has convinced us to believe that the observation of the intensity fluctuation correlation only takes place in the far-field zone of the thermal source. What will happen if we move the photodetectors D_1 and D_2 to the “near-field”, as shown in the unfolded schematic of Fig. 13? Does the theory of intensity fluctuation correlation still predict the point-to-point correlation in this situation? It is easy to see that in the near-field, (1) each photodetector, D_1 and D_2 , is able to receive radiation from a large number of sub-sources; and (2) D_1 and D_2 , have more chances to be triggered by radiation from different sub-sources. The ratio between the joint-detections triggered by radiation from a single sub-source and from different sub-sources is roughly $N/N^2 = 1/N$. For a large value of N the contribution of joint-detections triggered by radiation from a single sub-source is negligible comparing with $\bar{I}_1 \bar{I}_2$, and thus gives $\langle \Delta I_1 \Delta I_2 \rangle \sim 0$.

For half a century (1956-2006), it has been believed that the second-order correlation observed in the HBT experiment is a statistical correlation of intensity fluctuations and the second-order spatial correlation is observable in the far-field only. This “far-field only” misconception has ended fifty years after the discovery of HBT. In 2006, Scarcelli *et al.* demonstrated a near-field lensless ghost imaging experiment with chaotic light and published with a seemingly “unreasonable” title: “Can two-photon correlation of chaotic light be considered as correlation of intensity fluctuations?” [5] The experimental setup is similar to that of the historical HBT

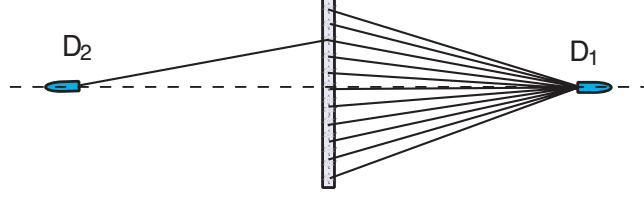


Figure 13: Modified near-field HBT measurement - a unfolded Klyshko picture of the setup. In near-field the “star” (source of thermal radiation) is more like a disk to D_1 and D_2 . Each point on the disk can be considered as an independent sub-source. It is easy to see that (1) D_1 and D_2 are capable of receiving radiation from a large number of sub-sources; and (2) D_1 and D_2 have more chances to be triggered by radiation from different sub-sources.

experiment, except in the near-field¹. The experimental result showed that the point-to-point second-order spatial correlation is observable in the near-field and is useful for reproducing ghost images in a nonlocal manner.²

In fact, far-field is not a necessary condition for observing the partial point-to-point correlation of thermal light from the view point of two-photon interference. Consider a radiation source that contains a large number of independent point sub-sources in the Fresnel near-field zone. The radiation fields $E(\mathbf{r}_1, t_1)$ and $E(\mathbf{r}_2, t_2)$ are the result of the superposition of the sub-fields that are excited by each of the independent sub-sources. The sub-fields are labeled as $E_j(\mathbf{r}_1, t_1)$ and $E_j(\mathbf{r}_2, t_2)$ in terms of the sub-sources, labeled by index j , and the photodetectors D_1 and D_2 , labeled by 1 and 2. The second-order mutual coherence function, or the second-order correlation function, is given by

$$\begin{aligned} \Gamma^{(2)}(\mathbf{r}_1, t_1; \mathbf{r}_2, t_2) &= \langle E^*(\mathbf{r}_1, t_1) E(\mathbf{r}_1, t_1) E^*(\mathbf{r}_2, t_2) E(\mathbf{r}_2, t_2) \rangle \\ &= \langle \sum_{j,k,l,m} E_j^*(\mathbf{r}_1, t_1) E_k(\mathbf{r}_1, t_1) E_l^*(\mathbf{r}_2, t_2) E_m(\mathbf{r}_2, t_2) \rangle, \end{aligned} \quad (26)$$

where j, k, l, m label the independent point sub-sources. Due to the chaotic nature of the independent sub-sources, after the ensemble average the only surviving terms in the summation are those with: (1) $j = k, l = m$, (2) $j = m, k = l$. Therefore, $\Gamma^{(2)}(\mathbf{r}_1, t_1; \mathbf{r}_2, t_2)$ reduces to the sum of the following two groups:

$$\begin{aligned} \Gamma^{(2)}(\mathbf{r}_1, t_1; \mathbf{r}_2, t_2) &= \langle \sum_j E_j^*(\mathbf{r}_1, t_1) E_j(\mathbf{r}_1, t_1) \sum_l E_l^*(\mathbf{r}_2, t_2) E_l(\mathbf{r}_2, t_2) \\ &\quad + \sum_j E_j^*(\mathbf{r}_1, t_1) E_j(\mathbf{r}_2, t_2) \sum_l E_l^*(\mathbf{r}_2, t_2) E_l(\mathbf{r}_1, t_1) \rangle \\ &= \langle \sum_j \sum_l |E_j(\mathbf{r}_1, t_1) E_l(\mathbf{r}_2, t_2) + E_l(\mathbf{r}_1, t_1) E_j(\mathbf{r}_2, t_2)|^2 \rangle, \end{aligned} \quad (27)$$

where the ensemble average has taken into account the random phases associated with each of the independent sub-sources. Notice, when claiming the surviving terms $j = m, k = l$, we have assumed that the random phases of the optical radiation fields are addable through the measurement of two distant independent photodetectors. This postulate is beyond classical measurement theory of light.

¹The concept of “near-field” was defined by Fresnel to be distinct from the Fraunhofer far-field. The Fresnel near-field is different from the “near-surface-field”, which considers a distance of few wavelengths from a surface.

²One would be tempted to ask: why was this simple move to a near-field measurement not even attempted for 50 years?

In Eq. (27), $\Gamma^{(2)}(\mathbf{r}_1, t_1; \mathbf{r}_2, t_2)$ is written as a superposition between the product of fields $E_j(\mathbf{r}_1, t_1)E_l(\mathbf{r}_2, t_2)$ and $E_l(\mathbf{r}_1, t_1)E_j(\mathbf{r}_2, t_2)$. The first term in the superposition corresponds to the situation in which the field at D_1 was generated by the j th sub-source, and the field at D_2 was generated by the l th sub-source. The second term in the superposition corresponds to a different but indistinguishable situation in which the field at D_1 was generated by the l th sub-source, and the field at D_2 was generated by the j th sub-source. Equation (27) indicates an interference phenomenon concealed in the joint measurement of D_1 and D_2 . This superposition physically occurs at two space-time points (\mathbf{r}_1, t_1) and (\mathbf{r}_2, t_2) by means of the joint-detection of D_1 and D_2 . This kind of interference has been called two-photon interference, which involves the superposition of two-photon amplitudes, a nonclassical entity corresponding to different yet indistinguishable alternative ways of triggering a joint-detection event in the quantum theory of photo-detection.

Before examining the physics of this peculiar interference, let us relate the second-order coherence function $\Gamma^{(2)}(\mathbf{r}_1, t_1; \mathbf{r}_2, t_2)$ with the first-order coherence functions,

$$\begin{aligned} \Gamma^{(2)}(\mathbf{r}_1, t_1; \mathbf{r}_2, t_2) &= \langle \sum_j \sum_l |E_j(\mathbf{r}_1, t_1)E_l(\mathbf{r}_2, t_2) + E_l(\mathbf{r}_1, t_1)E_j(\mathbf{r}_2, t_2)|^2 \rangle \\ &= \Gamma^{(1)}(\mathbf{r}_1, t_1; \mathbf{r}_1, t_1)\Gamma^{(1)}(\mathbf{r}_2, t_2; \mathbf{r}_2, t_2) + |\Gamma^{(1)}(\mathbf{r}_1, t_1; \mathbf{r}_2, t_2)|^2 \\ &= \Gamma_{11}^{(1)}\Gamma_{22}^{(1)} + \Gamma_{12}^{(1)}\Gamma_{21}^{(1)}, \end{aligned} \quad (28)$$

where we have defined the following shortened notations

$$\begin{aligned} \Gamma_{11}^{(1)} &= \langle \sum_j |E_j(\mathbf{r}_1, t_1)|^2 \rangle, \quad \Gamma_{22}^{(1)} = \langle \sum_l |E_l(\mathbf{r}_2, t_2)|^2 \rangle \\ \Gamma_{12}^{(1)} &= \langle \sum_j E_j^*(\mathbf{r}_1, t_1)E_j(\mathbf{r}_2, t_2) \rangle, \quad \Gamma_{21}^{(1)} = \langle \sum_l E_l(\mathbf{r}_1, t_1)E_l^*(\mathbf{r}_2, t_2) \rangle. \end{aligned}$$

Here, $\Gamma_{11}^{(1)}$ and $\Gamma_{22}^{(1)}$ represent, respectively, the expectation value of the intensity measured by D_1 and D_2 at space-time coordinates (\mathbf{r}_1, t_1) and (\mathbf{r}_2, t_2) , which include all contributions of the sub-intensities associated with each sub-source; $\Gamma_{12}^{(1)}$, which contains the “cross” terms between the sub-field and its conjugate at (\mathbf{r}_1, t_1) and (\mathbf{r}_2, t_2) , is the nontrivial contribution to the second-order correlation function $\Gamma^{(2)}(\mathbf{r}_1, t_1; \mathbf{r}_2, t_2)$. If the sub-fields are excited from N sub-sources, it is clear from Eq. (28) that the first and second summation group both have N^2 terms. The normalized degree of second-order coherence $\gamma^{(2)}(\mathbf{r}_1, t_1; \mathbf{r}_2, t_2)$ is related to the degree of first-order coherence by

$$\gamma^{(2)}(\mathbf{r}_1, t_1; \mathbf{r}_2, t_2) = \frac{\Gamma^{(2)}(\mathbf{r}_1, t_1; \mathbf{r}_2, t_2)}{\Gamma_{11}^{(1)}\Gamma_{22}^{(1)}} = 1 + |\gamma^{(1)}(\mathbf{r}_1, t_1; \mathbf{r}_2, t_2)|^2. \quad (29)$$

Equations (28) and (29) are valid for both the temporal and spatial coherence of chaotic light. For chaotic radiation, $\gamma^{(2)}(\mathbf{r}_1, t_1; \mathbf{r}_2, t_2)$ has a maximum value of two. Mathematically, we have related $\gamma^{(2)}(\mathbf{r}_1, t_1; \mathbf{r}_2, t_2)$ with $\gamma^{(1)}(\mathbf{r}_1, t_1; \mathbf{r}_2, t_2)$; however, $\gamma^{(1)}(\mathbf{r}_1, t_1; \mathbf{r}_2, t_2)$ in Eq. (29) is measured by two independent spatially separated photodetectors, which is physically different from the classic measurement of the first-order coherence function. This important physics cannot be ignored.

In the following we attempt a near-field calculation for the measurement of Scarcelli *et al* based on their modified near-field HBT experimental setup of Fig. 10. We start from Eq. (28)

$$\Gamma^{(2)}(\vec{\rho}_1, z_1; \vec{\rho}_2, z_2) = \langle \sum_j \sum_l |E_j(\vec{\rho}_1, z_1)E_l(\vec{\rho}_2, z_2) + E_l(\vec{\rho}_1, z_1)E_j(\vec{\rho}_2, z_2)|^2 \rangle, \quad (30)$$

where the indices j, l label each of the spatially distinguishable sub-sources. In the near-field we apply the Fresnel approximation as usual to propagate the field from each sub-source to the

photodetectors. Substituting the Green's functions into Eq. (30), $\Gamma^{(2)}(\vec{\rho}_1, z_1; \vec{\rho}_2, z_2)$ is formally written as

$$\begin{aligned} & \Gamma^{(2)}(\vec{\rho}_1, z_1; \vec{\rho}_2, z_2) \\ &= \langle \int d\vec{k} d\vec{k}' |g(\vec{\rho}_1, z_1, \vec{k})g(\vec{\rho}_2, z_2, \vec{k}') + g(\vec{\rho}_2, z_2, \vec{k})g(\vec{\rho}_1, z_1, \vec{k}')|^2 \rangle \\ &= \langle \int d\vec{k} |g(\vec{\rho}_1, z_1, \vec{k})|^2 \int d\vec{k}' |g(\vec{\rho}_2, z_2, \vec{k}')|^2 + \left| \int d\vec{k} g^*(\vec{\rho}_1, z_1, \vec{k}) g(\vec{\rho}_2, z_2, \vec{k}) \right|^2 \rangle. \end{aligned} \quad (31)$$

In Eq. (31) we have changed the order between the summation among the sub-sources and the integral of the transverse wavevectors. The summation of the sub-sources has been formally embedded into the Green's functions. Substituting the Green's function derived in Appendix A for free propagation

$$g(\vec{\rho}_j, z_j, \vec{k}) = \frac{-i\omega}{2\pi c} \frac{e^{i\frac{\omega}{c}z_j}}{z_j} \int d\vec{\rho}_0 a(\vec{\rho}_0) e^{i\varphi(\vec{\rho}_0)} e^{i\frac{\omega}{2cz_j}|\vec{\rho}_j - \vec{\rho}_0|^2}$$

into Eq. (31), we obtain $\Gamma_{11}^{(1)}\Gamma_{22}^{(1)} \sim \text{constant}$ and

$$\Gamma_{12}^{(1)}(\vec{\rho}_1, z_1; \vec{\rho}_2, z_2) \propto \langle \frac{1}{z_1 z_2} \int d\vec{\rho}_0 a^2(\vec{\rho}_0) e^{-i\frac{\omega}{c}z_1} e^{-i\frac{\omega}{2cz_1}|\vec{\rho}_1 - \vec{\rho}_0|^2} e^{i\frac{\omega}{c}z_2} e^{i\frac{\omega}{2cz_2}|\vec{\rho}_2 - \vec{\rho}_0|^2} \rangle.$$

Assuming $a^2(\vec{\rho}_0) \sim \text{constant}$, and taking $z_1 = z_2 = d$, we obtain

$$\begin{aligned} \Gamma_{12}^{(1)}(\vec{\rho}_1; \vec{\rho}_2) &\propto \int d\vec{\rho}_0 a^2(\vec{\rho}_0) e^{-i\frac{\omega}{2cd}|\vec{\rho}_1 - \vec{\rho}_0|^2} e^{i\frac{\omega}{2cd}|\vec{\rho}_2 - \vec{\rho}_0|^2} \\ &\propto e^{-i\frac{\omega}{2cd}(|\vec{\rho}_1|^2 - |\vec{\rho}_2|^2)} \int d\vec{\rho}_0 a^2(\vec{\rho}_0) e^{i\frac{\omega}{cd}(\vec{\rho}_1 - \vec{\rho}_2) \cdot \vec{\rho}_0} \\ &\propto e^{-i\frac{\omega}{2cd}(|\vec{\rho}_1|^2 - |\vec{\rho}_2|^2)} \text{somb}\left[\frac{R}{d} \frac{\omega}{c} |\vec{\rho}_1 - \vec{\rho}_2|\right], \end{aligned} \quad (32)$$

where we have assumed a disk-like light source with a finite radius of R . The second-order spatial correlation function $\Gamma^{(2)}(\vec{\rho}_1; \vec{\rho}_2)$ is thus

$$\Gamma^{(2)}(|\vec{\rho}_1 - \vec{\rho}_2|) = I_0^2 \left[1 + \left|\text{somb}\left(\frac{R}{d} \frac{\omega}{c} |\vec{\rho}_1 - \vec{\rho}_2|\right)\right|^2\right]. \quad (33)$$

Consequently, the degree of second-order spatial coherence is

$$\gamma^{(2)}(|\vec{\rho}_1 - \vec{\rho}_2|) = 1 + \left|\text{somb}\left(\frac{R}{d} \frac{\omega}{c} |\vec{\rho}_1 - \vec{\rho}_2|\right)\right|^2. \quad (34)$$

For a large value of $2R/d \sim \Delta\theta$, where $\Delta\theta$ is the angular size of the radiation source viewed at the photodetectors, the point-spread *somb*-function can be approximated as a δ -function of $|\vec{\rho}_1 - \vec{\rho}_2|$. We thus effectively have a ‘‘point-to-point’’ correlation between the transverse planes of $z_1 = z_0$ and $z_2 = z_0$. In the 1-D approximation, Eqs. (33) and (34) become

$$\Gamma^{(2)}(x_1 - x_2) = I_0^2 \left[1 + \text{sinc}^2\left(\frac{\pi\Delta\theta(x_1 - x_2)}{\lambda}\right)\right] \quad (35)$$

and

$$\gamma^{(2)}(x_1 - x_2) = 1 + \text{sinc}^2\left(\frac{\pi\Delta\theta(x_1 - x_2)}{\lambda}\right). \quad (36)$$

Equations (35) and (36) were confirmed experimentally by Scarcelli *et al.* in 2005 [6]. Figure 14 is the unfolded version of the experimental setup. By using a fairly large sized chaotic light source, $\Delta\theta \gg \lambda/D$, where D is the diameter of the source, the point-to-point correlation is

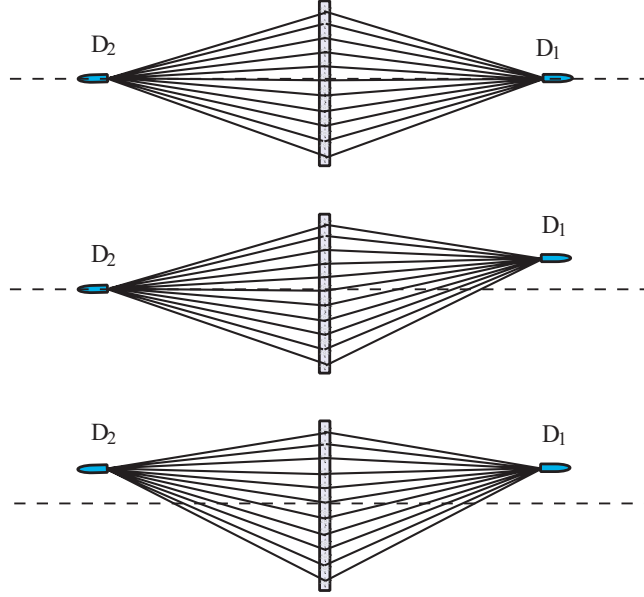


Figure 14: Near-field second-order spatial correlation measurement by Scarcelli *et al.* Upper: D_1 and D_2 are placed at equal distances from the source and aligned symmetrically on the optical axis, $\langle \Delta I_1 \Delta I_2 \rangle \sim \text{Maximum}$; Middle: D_1 is moved up to a non-symmetrical position, $\langle \Delta I_1 \Delta I_2 \rangle \sim 0$; Lower: D_2 is moved up to a symmetrical position with D_1 , $\langle \Delta I_1 \Delta I_2 \rangle \sim \text{Maximum}$, again. Notice, equal distance is required for observing the correlation.

observed when the two point-like-photodetectors, D_1 and D_2 , are aligned symmetrically in the near-field transverse planes, as indicated in the upper and lower cases of Fig. 14. In the upper measurement, D_1 and D_2 are aligned symmetrically on the optical axis. A *sinc*-like function of $\langle \Delta I_1 \Delta I_2 \rangle$ is observed by scanning either D_1 or D_2 transversely in the neighborhood of the optical axis. When D_1 is moved a few millimeters up (or down) from its symmetrical position, as shown in the middle figure, the correlation disappears, $\langle \Delta I_1 \Delta I_2 \rangle \sim 0$, by scanning either D_1 or D_2 . In the lower measurement D_2 is moved up (or down) to a symmetrical position, again with respect to D_1 . A similar *sinc*-like function of $\langle \Delta I_1 \Delta I_2 \rangle$ is observed by scanning either D_1 or D_2 in the neighborhood of their new symmetrical positions.

The observation is clearly an interference phenomenon. Unfortunately, this kind of interference is neither $|E_j + E_l|^2$ nor $|E_1 + E_2|^2$. The interference corresponds to $|E_{j1}E_{l2} + E_{l1}E_{j2}|^2$, which is schematically illustrated in Fig. 15. It is easy to find that all the amplitude pairs

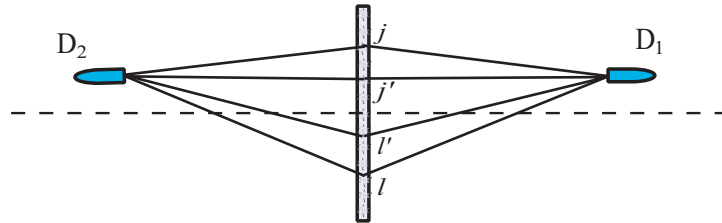


Figure 15: Schematic illustration of $\sum_{j,l} |E_{j1}E_{l2} + E_{l1}E_{j2}|^2$. It is clear that all amplitudes pairs $j1 \times l2$ and $l1 \times j2$, where j and l represent all sub-point-sources, are in phase and superposed constructively when D_1 and D_2 are located at $\vec{\rho}_1 = \vec{\rho}_2$.

$j1 \times l2$ and $l1 \times j2$, $j'1 \times l'2$ and $l'1 \times j'2$, $j1 \times l'2$ and $l'1 \times j2$, and $j'1 \times l2$ and $l1 \times j'2$, etc., are in phase, pair by pair, and thus superposed constructively while D_1 and D_2 are located at $\vec{\rho}_1 = \vec{\rho}_2$. Consequently, the summation of these interference terms will yield a maximum value. When $\vec{\rho}_1 \neq \vec{\rho}_2$, however, each pair may have a different relative phase and contribute different values to the summation, resulting in a constant value. It seems to make no sense to claim an interference between $[(E_j \text{ goes to } D_1) \times (E_l \text{ goes to } D_2)]$ and $[(E_l \text{ goes to } D_1) \times (E_j \text{ goes to } D_2)]$ in the framework of Maxwell's electromagnetic wave theory of light. This statement is more likely adapted from particle physics, and is more suitable to describe the behavior of particles: $[(\text{particle-}j \text{ goes to } D_1) \times (\text{particle-}l \text{ goes to } D_2)]$ and $[(\text{particle-}l \text{ goes to } D_1) \times (\text{particle-}j \text{ goes to } D_2)]$, rather than waves. Classical waves do not behave in such a way. On the other hand, the quantum theory of photo-detection [24] gives an adequate physical picture for this kind of interference: there exists two indistinguishable alternative ways of triggering a joint-detection event $[(\text{photon } j \text{ triggers } D_1) \times (\text{photon } l \text{ triggers } D_2)]$ and $[(\text{photon } l \text{ triggers } D_1) \times (\text{photon } j \text{ triggers } D_2)]$. The superposition takes place between these two quantum probability amplitudes.

It is worthwhile to emphasize that this kind of interference is not the interference between two photons, instead, it is the result of a superposition between two indistinguishable two-photon amplitudes, and is thus called *two-photon interference* [9].

The point-to-point correlation between the planes $z_1 = z_0$ and $z_2 = z_0$ of chaotic radiation was utilized by Scarcelli *et al.* in 2006 for reproducing “ghost” images [5]. Similar to classical imaging, the reproduction of the aperture function on the image plane is the result of the following convolution

$$R_{12} \propto \int_{\text{object}} d\vec{\rho}_2 |A(\vec{\rho}_2)|^2 [1 + |\text{somb}(\frac{R}{d} \frac{\omega}{c} |\vec{\rho}_1 - \vec{\rho}_2|)|^2] \quad (37)$$

in 2-D, or

$$R_{12} \propto \int_{\text{object}} dx_2 |A(x_2)|^2 [1 + \text{sinc}^2(\frac{\pi \Delta \theta (x_1 - x_2)}{\lambda})] \quad (38)$$

in 1-D. It is clear that the spatial resolution of the ghost image is determined by the angular diameter of the light source: the larger the size of the source in transverse dimensions, the higher the spatial resolution of the lensless ghost image.

The conceptual schematic setup of the near-field lensless ghost imaging experiment has been shown in Fig. 10. In the following we give a more detailed description of this experiment: radiation from a chaotic pseudothermal source [23] was equally divided into two optical paths by a 50%–50% non-polarizing beam-splitter. In arm *A* an object, a double-slit with slit separation $d = 1.5$ mm and slit width $a = 0.2$ mm, was placed at a distance $z_1 = 139$ mm from the source and a bucket detector (D_1) was placed just behind the object. In arm *B* a point detector D_2 was scanned in the transverse plane of $z_2 = z_1$. The correlation was measured by either a photon-counting coincidence circuit or by a standard HBT correlator. In the photon counting regime two Geiger mode avalanche photodiodes were employed for single-photon measurements. In the HBT scheme, the two photodetectors were silicon PIN photodiodes. The bucket detector D_1 was simulated by using a short focal length lens ($f = 25\text{mm}$) to focus the light onto the active area of the detector while the point detector D_2 was simulated by a pinhole. Figure 16(a) is an unfolded schematic of the experimental setup. Figure 16(b) reports the measured two-photon image of the double-slit. The result shows an equal-size reproduction of the double-slit when scanning photodetector D_2 along the x_2 axis. In Fig. 16(b) the DC background is subtracted from the image. Here we have made a 1-D scan to simplify the discussion.

To confirm that the observation is an imaged image, and not a “projection shadow”, Scarcelli *et al.* made two additional measurements. In the first measurement, photodetector D_1 was moved away from the ghost image plane of $z_1 = z_2$. Whether moved in the direction of $z_1 > z_2$

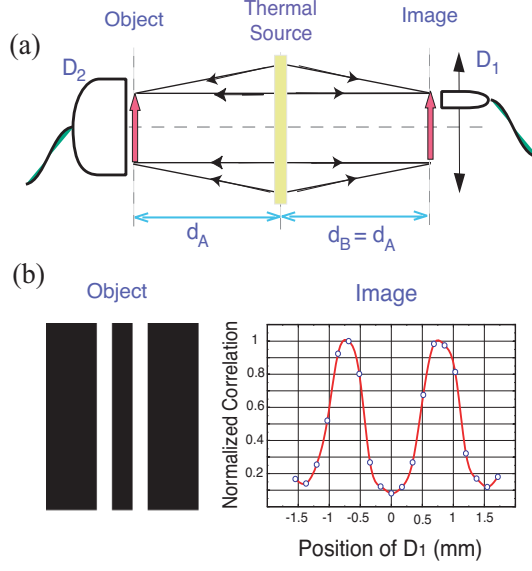


Figure 16: (a) Unfolded schematic of the near-field lensless ghost imaging experiment. (b) The double-slit and its ghost image. Notice, the DC constant has been subtracted from the correlation.

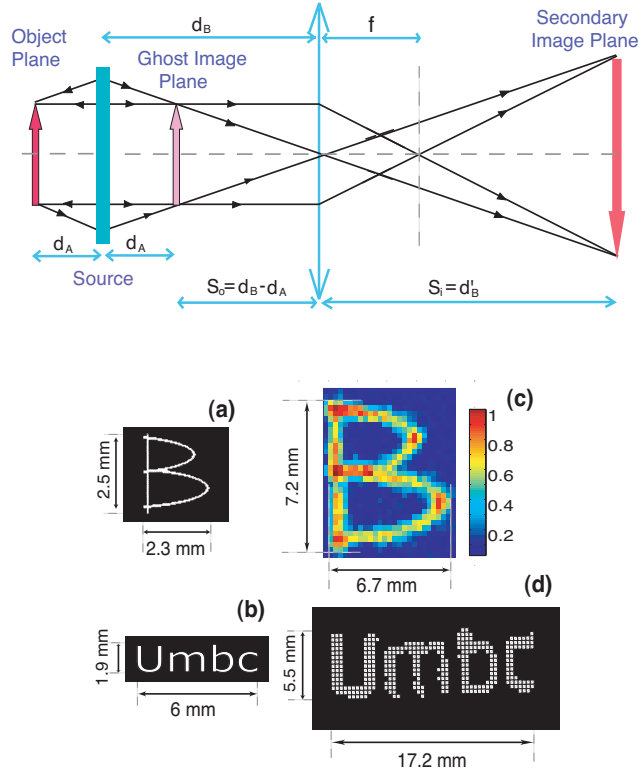


Figure 17: Unfolded schematic experimental setup of a secondary image measurement of the ghost image and the measured secondary images. By using a convex lens of focal length f , the ghost image is imaged onto a secondary image plane, which is defined by the Gaussian thin-lens equation, $1/s_o + 1/s_i = 1/f$.

or $z_1 < z_2$, the ghost image became “blurred”. The measurement also showed that the depth of the image is a function of the angular size of the thermal source: a larger source (larger values of R or $\Delta\theta$) produces sharper image with shorter depth, agreeing with Eqs. (37) and (38). In the second measurement, Scarcelli *et al.* constructed a secondary imaging system, illustrated in Fig. 17. By using a convex lens of focus length f the ghost image is imaged onto a secondary image plane. In this measurement the scanning photodetector D_1 is placed on the secondary imaging plane. The secondary image of the ghost image is observed in the joint-detection between D_1 and D_2 by means of either photon-counting coincidences or current-current correlation.

Meyers *et al.* have recently modified the near-field lensless ghost imaging of Scarcelli *et al.* into a new configuration of Fig. 4 [8]. Different from Scarcelli’s experiment and all other ghost imaging demonstrations, rather than measuring the transmitted light passing through a mask this setup reproduces the ghost image by counting the randomly *scattered* and *reflected* photons from the object. This new feature is not only useful for practical imaging-sensing field-applications, but also important from the viewpoint of fundamental concerns. In this experiment nothing is blocked-unblocked, it rejects the classical “projection shadow” model of ghost imaging in an undeniable way. Figure 18 shows the ghost image of a toy soldier model



Figure 18: Ghost image of a soldier toy model.

observed by Meyers *et al.* Although the image quality definitely needs to be improved it is pretty clear what the object is. The poor quality of the image is mainly due to the low photon-flux in the target-scattered light. There is no doubt that the observation is an image.

Although we have successfully calculated the ghost imaging by applying classical formalisms to nonlocal measurements, we cannot avoid to face the truth that the physics behind the calculation is two-photon interference. Implementing a calculation based on quantum mechanical formalism perhaps gives one more confidence in the quantum nature of the phenomenon. In fact, the quantum theory of thermal light ghost imaging is straightforward without any additional postulations beyond standard quantum theory of light. The second-order correlation has been given in Eq. (12) following the quantum theory of photo-detection [24]. What we need to do now is to define the state of the thermal radiation and to develop the operators of the fields. We assume a large number of atoms that are ready for two-level atomic transition. Most of the time, the atoms are in their ground state. There is, however, a small chance for each atom to be excited to a higher energy level E_2 ($\Delta E_2 \neq 0$) and later returns back to its ground state E_1 . It is reasonable to assume that each atomic transition generates a field in the following

single-photon state

$$|\Psi\rangle \simeq |0\rangle + \epsilon \sum_{\mathbf{k},s} f(\mathbf{k},s) \hat{a}_{\mathbf{k},s}^\dagger |0\rangle, \quad (39)$$

where $|\epsilon| \ll 1$ is the probability amplitude for the atomic transition, $f(\mathbf{k},s) = \langle \Psi_{\mathbf{k},s} | \Psi \rangle$ is the probability amplitude for the radiation field to be in the single-photon state of wave number \mathbf{k} and polarization s : $|\Psi_{\mathbf{k},s}\rangle = |1_{\mathbf{k},s}\rangle = \hat{a}_{\mathbf{k},s}^\dagger |0\rangle$. For this simplified two-level system, the density matrix that characterizes the state of the radiation field excited by a large number of possible atomic transitions is thus

$$\begin{aligned} \hat{\rho} &= \prod_{t_{0j}} \left\{ |0\rangle + \epsilon \sum_{\mathbf{k},s} f(\mathbf{k},s) e^{-i\omega t_{0j}} \hat{a}_{\mathbf{k},s}^\dagger |0\rangle \right\} \\ &\times \prod_{t_{0k}} \left\{ \langle 0| + \epsilon^* \sum_{\mathbf{k}',s'} f(\mathbf{k}',s') e^{i\omega' t_{0k}} \langle 0| \hat{a}_{\mathbf{k}',s'} \right\} \\ &\simeq \left\{ |0\rangle + \epsilon \left[\sum_{t_{0j}} \sum_{\mathbf{k},s} f(\mathbf{k},s) e^{-i\omega t_{0j}} \hat{a}_{\mathbf{k},s}^\dagger |0\rangle \right] + \epsilon^2 [\dots] \right\} \\ &\times \left\{ \langle 0| + \epsilon^* \left[\sum_{t_{0k}} \sum_{\mathbf{k}',s'} f(\mathbf{k}',s') e^{i\omega' t_{0k}} \langle 0| \hat{a}_{\mathbf{k}',s'} \right] + \epsilon^{*2} [\dots] \right\}, \end{aligned} \quad (40)$$

where $e^{-i\omega t_{0j}}$ is a random phase factor associated with the j th atomic transition. Since $|\epsilon| \ll 1$, it is a good approximation to keep the necessary lower-order terms of ϵ in Eq. (40). After summing over t_{0j} (t_{0k}) by taking all its possible values we obtain

$$\begin{aligned} \hat{\rho} &\simeq |0\rangle \langle 0| + |\epsilon|^2 \sum_{\mathbf{k},s} |f(\mathbf{k},s)|^2 |1_{\mathbf{k},s}\rangle \langle 1_{\mathbf{k},s}| \\ &+ |\epsilon|^4 \sum_{\mathbf{k},s} \sum_{\mathbf{k}',s'} |f(\mathbf{k},s)|^2 |f(\mathbf{k}',s')|^2 |1_{\mathbf{k},s} 1_{\mathbf{k}',s'}\rangle \langle 1_{\mathbf{k},s} 1_{\mathbf{k}',s'}| + \dots \end{aligned} \quad (41)$$

In the *photon counting* regime, it is reasonable to model the thermal light in terms of *single photon states*. Similar to our earlier discussion we will focus on the transverse correlation and assume the thermal radiation is monochromatic in Eq. (41),

$$\hat{\rho} \simeq |0\rangle \langle 0| + |\epsilon|^4 \sum_{\vec{\kappa}} \sum_{\vec{\kappa}'} \hat{a}^\dagger(\vec{\kappa}) \hat{a}^\dagger(\vec{\kappa}') |0\rangle \langle 0| \hat{a}(\vec{\kappa}') \hat{a}(\vec{\kappa}). \quad (42)$$

Basically we are modeling the light source as an incoherent statistical mixture of two photons with equal probability of having any transverse momentum $\vec{\kappa}$ and $\vec{\kappa}'$.

The spatial part of the second-order correlation function is

$$\begin{aligned} G^{(2)}(\vec{\rho}_1; \vec{\rho}_2) &= \text{tr}[\hat{\rho} E_1^{(-)}(\vec{\rho}_1) E_2^{(-)}(\vec{\rho}_2) E_2^{(+)}(\vec{\rho}_2) E_1^{(+)}(\vec{\rho}_1)] \\ &= \sum_{\vec{\kappa}, \vec{\kappa}'} \langle 1_{\vec{\kappa}} 1_{\vec{\kappa}'} | E_1^{(-)}(\vec{\rho}_1) E_2^{(-)}(\vec{\rho}_2) E_2^{(+)}(\vec{\rho}_2) E_1^{(+)}(\vec{\rho}_1) | 1_{\vec{\kappa}} 1_{\vec{\kappa}'} \rangle \\ &= \sum_{\vec{\kappa}, \vec{\kappa}'} |\langle 0 | E_2^{(+)}(\vec{\rho}_2) E_1^{(+)}(\vec{\rho}_1) | 1_{\vec{\kappa}} 1_{\vec{\kappa}'} \rangle|^2, \end{aligned} \quad (43)$$

again, $\vec{\rho}_j$ is the transverse coordinate of the j^{th} detector. The transverse part of the electric field operator can be written as

$$E_j^{(+)}(\vec{\rho}_j) \propto \sum_{\vec{\kappa}} g_j(\vec{\rho}_j; \vec{\kappa}) \hat{a}(\vec{\kappa}). \quad (44)$$

Substituting the field operators into Eq. (43) we have

$$G^{(2)}(\vec{\rho}_1; \vec{\rho}_2) = \sum_{\vec{\kappa}, \vec{\kappa}'} |g_2(\vec{\rho}_2, \vec{\kappa}) g_1(\vec{\rho}_1, \vec{\kappa}') + g_2(\vec{\rho}_2, \vec{\kappa}') g_1(\vec{\rho}_1, \vec{\kappa})|^2. \quad (45)$$

This expression represents the key result for our understanding of the phenomenon: it expresses an interference between two alternatives, different yet equivalent, which leads to a joint photodetection. The interference phenomenon is not, as in classical optics, due to the superposition of electromagnetic fields at a local point of space-time. It is due to the superposition of $g_2(\vec{\rho}_2, \vec{\kappa})g_1(\vec{\rho}_1, \vec{\kappa}')$ and $g_2(\vec{\rho}_2, \vec{\kappa}')g_1(\vec{\rho}_1, \vec{\kappa})$, the so-called two-photon amplitudes, non-classical entities that involve both arms of the optical setup as well as two distant photodetection events. Equation (45) can be further simplified as

$$\begin{aligned} G^{(2)}(\vec{\rho}_1; \vec{\rho}_2) &\propto \sum_{\vec{\kappa}} |g_1(\vec{\rho}_1, \vec{\kappa})|^2 \sum_{\vec{\kappa}'} |g_2(\vec{\rho}_2, \vec{\kappa}')|^2 + \left| \sum_{\vec{\kappa}} g_1^*(\vec{\rho}_1, \vec{\kappa}) g_2(\vec{\rho}_2, \vec{\kappa}) \right|^2 \\ &= G_{11}^{(1)}(\vec{\rho}_1) G_{22}^{(1)}(\vec{\rho}_2) + |G_{12}^{(1)}(\vec{\rho}_1; \vec{\rho}_2)|^2. \end{aligned} \quad (46)$$

In Eq. (46), we have formally linked $G^{(2)}$ with the first-order correlation functions of $G_{ij}^{(1)}$. The first term in Eq. (46) is the product of the mean intensities measured by the two detectors. The second term, which corresponds to the “intensity fluctuation correlation” in Eq. (25), is nothing but the two-photon interference term. The superposition takes place between the two-photon amplitudes $g_2(\vec{\rho}_2, \vec{\kappa})g_1(\vec{\rho}_1, \vec{\kappa}')$ and $g_2(\vec{\rho}_2, \vec{\kappa}')g_1(\vec{\rho}_1, \vec{\kappa})$.

We now calculate the $|G_{12}^{(1)}(\vec{\rho}_1; \vec{\rho}_2)|^2$ term of Eq. (46). With reference to the experimental setup of Fig. 10, the Green’s function of free-propagation is derived in Appendix A

$$\begin{aligned} g_1(\vec{\rho}_1; \vec{\kappa}) &= \int d\vec{\rho}_s \left\{ \frac{-i\omega}{2\pi c} \frac{e^{i\frac{\omega}{c}d_A}}{d_A} e^{i\frac{\omega}{2cd_A}|\vec{\rho}_1 - \vec{\rho}_s|^2} \right\} e^{-i\vec{\kappa} \cdot \vec{\rho}_s}, \\ g_2(\vec{\rho}_2; \vec{\kappa}) &= \int d\vec{\rho}_s' \left\{ \frac{-i\omega}{2\pi c} \frac{e^{i\frac{\omega}{c}d_B}}{d_B} e^{i\frac{\omega}{2cd_B}|\vec{\rho}_2 - \vec{\rho}_s'|^2} \right\} e^{-i\vec{\kappa} \cdot \vec{\rho}_s'}, \end{aligned}$$

where $\vec{\rho}_s$ is the transverse vector in the source plane, and the field has propagated from the source to the $\vec{\rho}_1$ plane and $\vec{\rho}_2$ plane in arms A and B, respectively.

Substituting $g_1^*(\vec{\rho}_1, \vec{\kappa})$ and $g_2(\vec{\rho}_2, \vec{\kappa})$ into $G_{12}^{(1)}(\vec{\rho}_1; \vec{\rho}_2)$ and completing the integral on $d\vec{\kappa}$, we obtain

$$\begin{aligned} G_{12}^{(1)}(\vec{\rho}_1; \vec{\rho}_2) &= \int d\vec{\kappa} g_1^*(\vec{\rho}_1, \vec{\kappa}) g_2(\vec{\rho}_2, \vec{\kappa}) \\ &\propto \int d\vec{\rho}_s e^{-i\frac{\omega}{c}d_A} e^{-i\frac{\omega}{2cd_A}|\vec{\rho}_1 - \vec{\rho}_s|^2} e^{i\frac{\omega}{c}d_B} e^{i\frac{\omega}{2cd_B}|\vec{\rho}_2 - \vec{\rho}_s|^2}. \end{aligned} \quad (47)$$

If we choose the distances from the source to the two detectors to be equal ($d_A = d_B = d$), the integral of $d\vec{\rho}_s$ in Eq. (47) yields a point-to-point correlation,

$$G_{12}^{(1)}(\vec{\rho}_1; \vec{\rho}_2) \propto \int d\vec{\rho}_s e^{i\frac{\omega}{cd}(\vec{\rho}_1 - \vec{\rho}_2) \cdot \vec{\rho}_s} = \text{somb}\left[\frac{R\omega}{d} \frac{c}{c} |\vec{\rho}_1 - \vec{\rho}_2|\right] \sim \delta(\vec{\rho}_1 - \vec{\rho}_2), \quad (48)$$

where the δ -function may apply by integrating $d\vec{\rho}_s$ on the source plane to infinity. The joint-detection counting rate between the scanning point detector D_1 and the fixed bucket detector D_2 is thus

$$R_c(\vec{\rho}_1) \propto \int d\vec{\rho}_2 |A(\vec{\rho}_2)|^2 [G_{11}^{(1)} G_{22}^{(1)} + |G_{12}^{(1)}(\vec{\rho}_1; \vec{\rho}_2)|^2] \sim R_0 + |A(\vec{\rho}_1)|^2, \quad (49)$$

where R_0 is a constant and $A(\vec{\rho}_2)$ is the aperture function of the object.

We have successfully derived an analytical solution of ghost imaging with thermal radiation at single-photon approximation. It is clear that the partial point-to-point correlation of thermal radiation is the result of a constructive-destructive interference caused by the nonlocal superposition of two-photon amplitudes.

In fact, the quantum formalism is not restricted to single-photon states. The partial point-to-point correlation of $G^{(2)}(\vec{\rho}_1; \vec{\rho}_2)$ is generally true for any intensity of thermal radiation [27].

The following calculation is valid for an arbitrary quantized thermal field with occupation number from $n_{\mathbf{k},s} = 0$ to $n_{\mathbf{k},s} \gg 1$. In this calculation we keep all higher order terms in Eq. (40). After summing over t_{0j} and t_{0k} the density matrix can be written as

$$\hat{\rho} = \sum_{\{n\}} p_{\{n\}} |\{n\}\rangle \langle \{n\}|, \quad (50)$$

where $p_{\{n\}}$ is the probability for the thermal field to be in the state

$$|\{n\}\rangle \equiv \prod_{\mathbf{k},s} |n_{\mathbf{k},s}\rangle = |n_{\mathbf{k}},s\rangle |n_{\mathbf{k}',s'}\rangle \dots |n_{\mathbf{k}''\dots',s''\dots'}\rangle.$$

The summation of Eq. (50) includes all possible mode \mathbf{k} , polarization s , and occupation number $n_{\mathbf{k},s}$ for the mode \mathbf{k} and polarization s . Substituting the field operators and the density operator of Eq. (50) into Eq. (43) we obtain the point-to-point correlation function at the two planes $z_1 = d$ and $z_2 = d$,

$$\begin{aligned} & G^{(2)}(\vec{\rho}_1; \vec{\rho}_2) \\ &= \sum_{\{n\}} \int d\vec{\kappa} \int d\vec{\kappa}' \int d\vec{\kappa}'' \int d\vec{\kappa}''' g_1^*(\vec{\kappa}, \vec{\rho}_1) g_2^*(\vec{\kappa}', \vec{\rho}_2) g_2(\vec{\kappa}'', \vec{\rho}_2) g_1(\vec{\kappa}''', \vec{\rho}_1) \\ & \quad \times p_{\{n\}} \langle \{n\} | a(\vec{\kappa}) a(\vec{\kappa}') a^\dagger(\vec{\kappa}'') a^\dagger(\vec{\kappa}''') | \{n\} \rangle \\ & \propto \sum_{\{n\}} n_{\vec{\kappa}} n_{\vec{\kappa}'} \int d\vec{\kappa} \int d\vec{\kappa}' \int d\vec{\kappa}'' \int d\vec{\kappa}''' g_1^*(\vec{\kappa}, \vec{\rho}_1) g_2^*(\vec{\kappa}', \vec{\rho}_2) g_2(\vec{\kappa}'', \vec{\rho}_2) g_1(\vec{\kappa}''', \vec{\rho}_1) \\ & \quad \times p_{\{n\}} (\delta_{\vec{\kappa}\vec{\kappa}'''} \delta_{\vec{\kappa}'\vec{\kappa}''} + \delta_{\vec{\kappa}\vec{\kappa}''} \delta_{\vec{\kappa}'\vec{\kappa}'''}) \\ &= \sum_{\substack{\{n\} \\ n_{\vec{\kappa}} n_{\vec{\kappa}'} \\ n_{\vec{\kappa}''} n_{\vec{\kappa}'''}}} p_{\{n\}} n_{\vec{\kappa}} n_{\vec{\kappa}'} \left\{ \int d\vec{\kappa} \int d\vec{\kappa}' \frac{1}{2} |g_1(\vec{\kappa}, \vec{\rho}_1) g_2(\vec{\kappa}', \vec{\rho}_2) + g_2(\vec{\kappa}, \vec{\rho}_2) g_1(\vec{\kappa}', \vec{\rho}_1)|^2 \right\} \\ & \propto \left\{ 1 + \text{somb}^2 \left[\frac{R}{d} \frac{\omega}{c} (\vec{\rho}_1 - \vec{\rho}_2) \right] \right\}, \end{aligned} \quad (51)$$

where monochromatic radiation and single polarization are assumed for simplicity. As shown in Eq. (51), the partial point-to-point correlation of thermal light at any intensity is the result of a constructive-destructive interference between two quantum-mechanical amplitudes, corresponding to different yet indistinguishable alternatives of triggering a photocurrent-photocurrent correlation between two spatially separated photodetectors D_1 and D_2 . It is also interesting to see from Eq. (51) that this partial point-to-point correlation is independent of the occupation numbers, $\{n\}$, and spectral probability distribution, $p_{\{n\}}$, of the quantized thermal radiation.

5 Quantum? Classical?

After the discussion and clarification of the concepts of ghost imaging we are ready to answer whether ghost imaging is a quantum phenomenon or a trivial classical statistical correlation of intensity fluctuations. It is clear that the classical statistical model of intensity fluctuations would not work for type-one ghost imaging. In Eq. (20), the intensity-intensity correlation function between the object plane and the image plane is given by

$$\langle I_1 I_2 \rangle = \bar{I}_1 \bar{I}_2 + \langle \Delta I_1 \Delta I_2 \rangle = \text{somb}^2 \left(\frac{R}{s_o} \frac{\omega}{c} \left| \vec{\rho}_1 + \frac{\vec{\rho}_2}{m} \right| \right).$$

Based on the classical concept of statistical correlations of intensity fluctuations, in this case the mean intensities, \bar{I}_1 and \bar{I}_2 must be zero, otherwise the result would lead to non-physical conclusions. The measurements, however, never yield zero mean values of \bar{I}_1 and \bar{I}_2 under any

circumstances. Moreover, the calculation has shown that the point-to-point image-forming correlation is the result of a constructive-destructive interference between two-photon amplitudes, representing a quantum phenomenon.

Type-two ghost imaging is based on the partial point-to-point correlation of thermal radiation between the near-field object-image planes. The far-field partial point-to-point correlation of thermal light was discovered in 1956 and was successfully interpreted as the classical statistical correlation of intensity fluctuations. The classical theory, however, cannot give a convincing interpretation for the near-field ghost imaging experiment of Scarcelli *et al* [5]. In the near-field, the photodetectors, D_1 and D_2 , both receive a large number of independent spatial modes that correspond to a large number of independent point sub-sources of the thermal radiation. Due to the chaotic nature of the source it is easy to see that $\langle \Delta I_1 \Delta I_2 \rangle = 0$ in this case. In half a century, we have been misled by the intensity fluctuation correlation theory to believe that the HBT correlation of thermal light only occurs in far-field. It was not until 2006, 50 years after the discovery of HBT, that Scarcelli *et al* simply moved D_1 and D_2 to the near-field and utilized the near-field point-to-point correlation of thermal light for ghost imaging. What is the true physics behind the phenomenon? We have found that the near-field point-to-point correlation of thermal radiation is the result of an interference between two-photon amplitudes. Unfortunately, the concept of two-photon interference has no counterpart in Maxwell's electromagnetic theory of light. The concept belongs to quantum mechanics.

It is because of this peculiar nonlocal interference, which results in the point-to-point image-forming correlation between the object and image planes, that we consider the type-one and type-two ghost imaging quantum phenomenon.

5.1 Ghost image? Ghost shadow?

It is worthwhile emphasizing that the above conclusion is applicable to ghost *imaging*, but not to ghost *shadow projection* (or any other different type of correlation measurement). For instance, an interesting experiment on ghost “imaging” was demonstrated by Gatti *et al* to support their classical view point on this subject. Their experimental setup is depicted in Fig. 19 [11]. Indeed, their observation can be interpreted classically. To understand why the effect is classical and, above all, how it differs from a true ghost image, let us find out how their ghost shadow was created in the coincidence counting rate. There are three key points to understanding this experiment. (1) Due to the entangled nature of the two-photon source, a signal-idler pair is always emitted from the same point in the output plane of the SPDC. (2) The object mask and the output plane of the SPDC crystal almost coincide. (3) The use of the lens L ($Z = 2f$) forces a classical point-to-point relationship between the output plane of the source and the plane of the CCD (the CCD is represented in Fig. 19 by the scanning detector D_I); in other words, the lens makes a *classical* image of the source by the idler beam at the CCD plane. Whenever a signal photon is not blocked by the object mask (the double-slit in the arm of the Bucket detector) a coincidence occurs between the bucket detector D_s and the CCD element receiving the image of the source point where the signal-idler pair is released. However, if a signal photon is blocked by the object mask, there would obviously be no joint-detection between the bucket detector D_s and the corresponding CCD element. A shadow of the object mask is thus reconstructed in coincidences. It is interesting to see that a point-to-point correspondence exists in this experiment; however, this point-to-point relation is between the output plane of the source and its “classical image” plane, rather than between the object and the ghost image planes. This point-to-point correspondence results in a classical image of the light source which is fundamentally different from the point-to-point image-forming correlation required in the ghost imaging experiments. The use of entangled photon pairs in this experiment cannot change the classical nature of the observed effect. It is not surprising that this kind of experimental setup leads to the classical perspective of the authors on the subject of ghost “imaging” [25].

To convince ourselves of the purely classical nature of the ghost shadow/projection, suffice

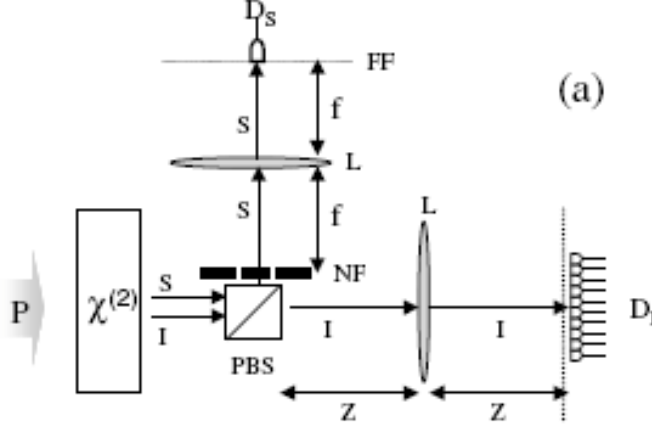


Figure 19: Schematic ghost “imaging” setup of Gatti *et al.* with entangled photon pairs of SPDC. The use of the lens L ($Z = 2f$) forces a classical point-to-point relationship between the output plane of the source and the plane of the CCD (the CCD is represented in this figure by the scanning detector D_I), i.e., a *classical* image of the source is made by the idler beam at the CCD plane. Whenever a signal photon is not blocked by the object mask (the double-slit in the bucket detector arm) a coincidence occurs between the bucket detector D_s and the CCD element receiving the image of its idler twin. However, if a signal photon is blocked by the object mask, there would obviously be no joint-detection between the bucket detector D_s and the CCD element receiving the image of its idler twin. A shadow of the object mask is thus reconstructed in coincidences. It is interesting to see that a point-to-point correspondence exists in this experiment; however, this point-to-point relation is between the output plane of the source and its “classical image” plane, rather than between the object and the ghost image planes. The use of entangled photon pairs in this experiment cannot change its classical nature of shadow projection.

it to realize that the same effect can be obtained by substituting the two-photon source of SPDC with a large number of point thermal sources, which are turned on one at a time. In this case, the ghost shadow is still observable in the experimental setup of Gatti *et al.* This kind of arguments, as well as the classical perspective of Gatti *et al.*, would not work for a true ghost imaging experiment.

Using the same setup, Gatti *et al.* also performed measurements with thermal radiation rather than the entangled photon pair of SPDC [26]. The experimental result was used by Gatti *et al.* to support their classical intensity fluctuation correlation argument on the subject [25]. Again, different from ghost imaging in which the point-to-point image-forming correlation occurs between the object and ghost image planes, this experiment produces a point-to-point correlation between the source plane and the classical image plane of the source by the $2f - 2f$ lens-system. The lens L images each of the “speckles” of a chaotic light source onto a CCD when z was chosen to be twice the focal length, $z = 2f$, in other words, each element of the CCD receives the thermal radiation from a unique speckle on the source plane. Due to the almost “null” distance between the object mask and the thermal source, the blocking-unblocking of the speckles by the mask will create a shadow of the object mask at the plane of the CCD by measuring joint-detections with the bucket detector D_s . A joint-detection event can be created either by a single speckle or by different speckles. The radiation from an unblocked speckle (in the arm of the bucket detector) propagates and focuses onto the photodetector D_s and may give rise to a joint-detection with the classical image of the same speckle produced by the $2f - 2f$ lens-system on the CCD. An “unblocked” speckle gives rise to a non-zero correlation of the intensity

fluctuations, $\langle \Delta I_1 \Delta I_2 \rangle \neq 0$, in the joint-detection event between a unique CCD element which receives the classical image of that speckle and the bucket photodetector D_s (triggered by the same speckle). If a speckle is blocked by the object mask before reaching the bucket detector D_s , obviously there would be no chance for that speckle to produce a joint-detection event with a corresponding CCD element so its contribution to the intensity fluctuation correlation will be zero, ($\langle \Delta I_1 \Delta I_2 \rangle = 0$). A shadow of the object mask is then reconstructed in coincidences. Of course, there are still chances to have joint-detections between the CCD element which receives the image of that blocked speckle (reminder: the “blocking-unblocking” is in the D_s arm), and the bucket detector D_s that is triggered by other unblocked speckles. These joint-detections produced by “wrong” speckle pairs will contribute to the constant background $\bar{I}_1 \bar{I}_2$.

This experiment is physically different from Scarcelli’s near-field lensless ghost imaging experiment. Scarcelli *et al.* produced ghost *images* by means of a point-to-point image-forming correlation between the object and ghost image planes, which is the result of a two-photon constructive-destructive interference effect. However, in the experiment of Gatti *et al.*, the point-to-point correspondence occurs between the plane of the source and the plane where a classical image of the source is reconstructed by the $2f - 2f$ system. The object only plays the role of blocking-unblocking the speckles of the thermal source.

It is true that the classical theory of the statistical correlation of intensity fluctuations provides a reasonable interpretation to the experiment of Gatti *et al.* However, the same theory is not applicable to a different experimental situation such as the near-field lensless ghost imaging experiment of Scarcelli *et al.* Quantum? Classical? Clarification of the differences between the ghost imaging setups and other types of correlation measurements, such as ghost shadow/projection, could be the key to understanding the reasons behind the different opinions on the subject.

5.2 Local? Nonlocal?

We have discussed the physics of both type-one and type-two ghost imaging. Although different radiation sources are used for different cases, these two types of experiments demonstrated a similar point-to-point image-forming correlation:

Type-one:

$$\delta(\vec{\rho}_1 - \vec{\rho}_2) \sim \left| \int d\vec{\kappa}_s d\vec{\kappa}_i \delta(\vec{\kappa}_s + \vec{\kappa}_i) g_1(\vec{\kappa}_s, \vec{\rho}_1) g_2(\vec{\kappa}_i, \vec{\rho}_2) \right|^2, \quad (52)$$

Type-two:

$$\begin{aligned} 1 + \delta(\vec{\rho}_1 - \vec{\rho}_2) &\propto \left\langle \sum_j \sum_l |E_j(\vec{\rho}_1) E_l(\vec{\rho}_2) + E_l(\vec{\rho}_1) E_j(\vec{\rho}_2)|^2 \right\rangle \\ &= \left\langle \int d\vec{\kappa} d\vec{\kappa}' |g_1(\vec{\kappa}, \vec{\rho}_1) g_2(\vec{\kappa}', \vec{\rho}_2) + g_2(\vec{\kappa}, \vec{\rho}_2) g_1(\vec{\kappa}', \vec{\rho}_1)|^2 \right\rangle. \end{aligned} \quad (53)$$

Equations (52) and (53) indicate that the point-to-point correlation of ghost imaging, either type-one or type-two, are the results of two-photon superposition. Unfortunately, neither of them is in the form of $|\sum_j E_j|^2$ or $|E_1 + E_2|^2$, and neither is measured at a local space-time point. The interference shown in Eqs. (52) and (53) occurs at different space-time points through the coincidence measurement of two spatially separated independent photodetectors.

In type-one ghost imaging, the δ -function in Eq. (52) means a typical EPR position-position correlation of an entangled photon pair. In EPR’s language: when the pair is generated at the source the momentum and position of neither photon is determined, and neither photon-one nor photon-two “knows” where to go; however, if one of them is observed at a point at the object plane the other one must be found at a unique point in the image plane. In type-two ghost imaging, although the position-position determination in Eq. (53) is only partial,

it generates more surprises because of the chaotic nature of the radiation source. Photon-one and photon-two, emitted from a thermal source, are completely random and independent, i.e., both propagate freely to any direction and may arrive at any position in the object and image planes. Where does this partial correlation come from? If one insists the view point of intensity fluctuation correlation, then, it is reasonable to ask why the intensities of the two light beams exhibit fluctuation correlations at $\vec{\rho}_1 = \vec{\rho}_2$ only? Recall that in the experiment of Scarcelli *et al.* the ghost image is measured in near-field. Regardless of position, D_1 and D_2 receive light from all (a large number) point sub-sources of the thermal source, and all sub-sources fluctuate randomly and independently. If $\Delta I_1 \Delta I_2 = 0$ for $\vec{\rho}_1 \neq \vec{\rho}_2$, what is the physics to have $\Delta I_1 \Delta I_2 \neq 0$ at $\vec{\rho}_1 = \vec{\rho}_2$?

For 50 years, we have believed the point-to-point correlation of a thermal field is a trivial classical correlation phenomenon. In fact, this point-to-point correlation is *observed in* the intensity fluctuations, however, it is *not caused by* the intensity fluctuations. The point-to-point correlation is the result of a constructive-destructive interference due to the nonlocal superposition of two-photon amplitudes. The use of “classical light” in type-two ghost imaging cannot change the *nonlocal* interference nature of the phenomenon; the same as the use of entangled photon pairs cannot change the classical nature of the ghost shadow experiment of Gatti *et al.*

The classical superposition is considered “local”. The Maxwell electromagnetic field theory requires the superposition of the electromagnetic fields, either $|\sum_j E_j|^2$ or $|E_1 + E_2|^2$, takes place at a single space-time point (\mathbf{r}, t) . However, the superposition shown in Eqs. (52) and (53) happens at two different space-time points (\mathbf{r}_1, t_1) and (\mathbf{r}_2, t_2) and is measured by two independent photodetectors. Experimentally, it is not difficult to make the two photo-detection events space-like separated events. Following the definition given by EPR-Bell, we consider the superposition appearing in Eqs. (52) and (53) *nonlocal*. Although the two-photon interference of thermal light can be written and calculated in terms of classical formalism, the nonlocal superposition appearing in Eq. (53) has no counterpart in the classical measurement theory of light, unless one forces a nonlocal classical theory by allowing the superposition to occur at a distance through the measurement of independent photodetectors, as we have done in Eq. (27). Perhaps, it would be more difficult to accept a nonlocal classical measurement theory of thermal light rather than to apply a quantum mechanical concept to “classical” thermal radiation.

Acknowledgment: The author thanks M. D’Angelo, G. Scarcelli, J.M. Wen, T.B. Pittman, M.H. Rubin, and L.A. Wu for helpful discussions. This work is partially supported by AFOSR and ARO-MURI program.

Appendix A: Fresnel propagation

We are interested in knowing how a known field $E(\mathbf{r}_0, t_0)$ on the plane $z_0 = 0$ propagates or diffracts into $E(\mathbf{r}, t)$ on another plane $z = \text{constant}$. We assume the field $E(\mathbf{r}_0, t_0)$ is excited by an arbitrary source, either point-like or spatially extended. The observation plane of $z = \text{constant}$ is located at an arbitrary distance from plane $z_0 = 0$, either far-field or near-field. Our goal is to find out a general solution $E(\mathbf{r}, t)$, or $I(\mathbf{r}, t)$, on the observation plane, based on our knowledge of $E(\mathbf{r}_0, t_0)$ and the laws of the Maxwell electromagnetic wave theory. It is not easy to find such a general solution. However, the use of the Green’s function or the field transfer function, which describes the propagation of each mode from the plane of $z_0 = 0$ to the observation plane of $z = \text{constant}$, makes this goal formally achievable.

Unless $E(\mathbf{r}_0, t_0)$ is a non-analytic function in the space-time region of interest, there must

exist a Fourier integral representation for $E(\mathbf{r}_0, t_0)$

$$E(\mathbf{r}_0, t_0) = \int d\mathbf{k} E(\mathbf{k}) w_{\mathbf{k}}(\mathbf{r}_0, t_0) e^{-i\omega t_0}, \quad (A-1)$$

where $w_{\mathbf{k}}(\mathbf{r}_0, t_0)$ is a solution of the Helmholtz wave equation under appropriate boundary conditions. The solution of the Maxwell wave equation $w_{\mathbf{k}}(\mathbf{r}_0, t_0) e^{-i\omega t_0}$, namely the Fourier mode, can be a set of plane-waves or spherical-waves depending on the chosen boundary condition. In Eq. (A-1), $E(\mathbf{k}) = a(\mathbf{k})e^{i\varphi(\mathbf{k})}$ is the complex amplitude of the Fourier mode \mathbf{k} . In principle we should be able to find an appropriate Green's function which propagates each mode under the Fourier integral point by point from the plane of $z_0 = 0$ to the plane of observation,

$$\begin{aligned} E(\mathbf{r}, t) &= \int d\mathbf{k} E(\mathbf{k}) g(\mathbf{k}, \mathbf{r} - \mathbf{r}_0, t - t_0) w_{\mathbf{k}}(\mathbf{r}_0, t_0) e^{-i\omega t_0} \\ &= \int d\mathbf{k} g(\mathbf{k}, \mathbf{r} - \mathbf{r}_0, t - t_0) E(\mathbf{k}, \mathbf{r}_0, t_0), \end{aligned} \quad (A-2)$$

where $E(\mathbf{k}, \mathbf{r}_0, t_0) = E(\mathbf{k}) w_{\mathbf{k}}(\mathbf{r}_0, t_0) e^{-i\omega t_0}$. The secondary wavelets that originated from each point on the plane of $z_0 = 0$ are then superposed *coherently* on each point on the observation plane with their after-propagation amplitudes and phases. It is convenient to write Eq. (A-2) in the following form

$$E(\vec{\rho}, z, t) = \int d\omega d\vec{\kappa} g(\vec{\kappa}, \omega; \vec{\rho} - \vec{\rho}_0, z - z_0, t - t_0) E(\vec{\kappa}, \omega; \vec{\rho}_0, z_0, t_0), \quad (A-3)$$

where we have used the transverse-longitudinal coordinates in space-time ($\vec{\rho}$ and z) and in momentum ($\vec{\kappa}, \omega$).

Fig. A-1 is a simple example in which the field propagates freely from a finite size aperture A on the plane σ_0 to the observation plane σ . Based on Fig. A-1 we evaluate $g(\vec{\kappa}, \omega; \vec{\rho}, z)$, namely the Green's function for free-space Fresnel propagation-diffraction.

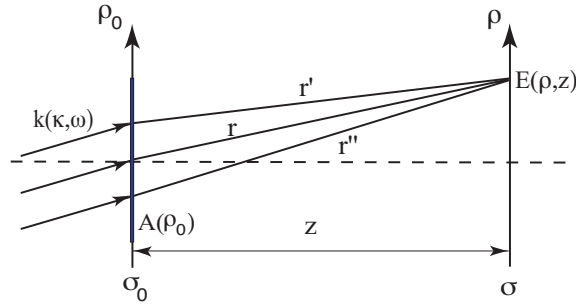


Figure A-1: Schematic of free-space Fresnel propagation. The complex amplitude $\tilde{A}(\vec{\rho}_0)$ is composed of a real function $A(\vec{\rho}_0)$ and a phase $e^{-i\vec{\kappa} \cdot \vec{\rho}_0}$ associated with each of the transverse wavevectors $\vec{\kappa}$ in the plane of σ_0 . Notice: only one mode of wavevector $\mathbf{k}(\vec{\kappa}, \omega)$ is shown in the figure.

According to the Huygens-Fresnel principle the field at a given space-time point $(\vec{\rho}, z, t)$ is the result of a superposition of the spherical secondary wavelets that originated from each point on the σ_0 plane (see Fig. A-1),

$$E(\vec{\rho}, z, t) = \int d\omega d\vec{\kappa} E(\vec{\kappa}, \omega; 0, 0) \int_{\sigma_0} d\vec{\rho}_0 \frac{\tilde{A}(\vec{\rho}_0)}{r} e^{-i(\omega t - \kappa r)}, \quad (A-4)$$

where we have set $z_0 = 0$ and $t_0 = 0$ at plane σ_0 , and defined $r = \sqrt{z^2 + |\vec{\rho} - \vec{\rho}_0|^2}$. In Eq. (A-4), $\tilde{A}(\vec{\rho}_0)$ is the complex amplitude or relative distribution of the field on the plane of

σ_0 , which may be written as a simple aperture function in terms of the transverse coordinate $\vec{\rho}_0$, as we have done in the earlier discussions.

In the near-field Fresnel paraxial approximation, when $|\vec{\rho} - \vec{\rho}_0|^2 \ll z^2$ we take the first-order expansion of r in terms of z and $\vec{\rho}$,

$$r = \sqrt{z^2 + |\vec{\rho} - \vec{\rho}_0|^2} \simeq z \left(1 + \frac{|\vec{\rho} - \vec{\rho}_0|^2}{2z^2}\right), \quad (A-5)$$

so that $E(\vec{\rho}, z, t)$ can be approximated as

$$E(\vec{\rho}, z, t) \simeq \int d\omega d\vec{\kappa} E(\vec{\kappa}, \omega, 0, 0) \int d\vec{\rho}_0 \frac{\tilde{A}(\vec{\rho}_0)}{z} e^{i\frac{\omega}{c}z} e^{i\frac{\omega}{2cz}|\vec{\rho} - \vec{\rho}_0|^2} e^{-i\omega t},$$

where $e^{i\frac{\omega}{2cz}|\vec{\rho} - \vec{\rho}_0|^2}$ is named the Fresnel phase factor.

Assuming that the complex amplitude $\tilde{A}(\vec{\rho}_0)$ is composed of a real function $A(\vec{\rho}_0)$ and a phase $e^{-i\vec{\kappa} \cdot \vec{\rho}_0}$, associated with the transverse wavevector and the transverse coordinate on the plane of σ_0 , as is reasonable for the setup of Fig. A-1, we can then write $E(\vec{\rho}, z, t)$ in the form

$$\begin{aligned} E(\vec{\rho}, z, t) &= \int d\omega d\vec{\kappa} E(\vec{\kappa}, \omega; 0, 0) e^{-i\omega t} \frac{e^{i\frac{\omega}{c}z}}{z} \int d\vec{\rho}_0 \tilde{A}(\vec{\rho}_0) e^{i\vec{\kappa} \cdot \vec{\rho}_0} e^{i\frac{\omega}{2cz}|\vec{\rho} - \vec{\rho}_0|^2}. \end{aligned}$$

The Green's function $g(\vec{\kappa}, \omega; \vec{\rho}, z)$ for free-space Fresnel propagation is thus

$$g(\vec{\kappa}, \omega; \vec{\rho}, z) = \frac{e^{i\frac{\omega}{c}z}}{z} \int_{\sigma_0} d\vec{\rho}_0 \tilde{A}(\vec{\rho}_0) e^{i\vec{\kappa} \cdot \vec{\rho}_0} G(|\vec{\rho} - \vec{\rho}_0|, \frac{\omega}{cz}). \quad (A-6)$$

In Eq. (A-6) we have defined a Gaussian function $G(|\vec{\alpha}|, \beta) = e^{i(\beta/2)|\alpha|^2}$, namely the Fresnel phase factor. It is straightforward to find that the Gaussian function $G(|\vec{\alpha}|, \beta)$ has the following properties:

$$\begin{aligned} G^*(|\vec{\alpha}|, \beta) &= G(|\vec{\alpha}|, -\beta), \\ G(|\vec{\alpha}|, \beta_1 + \beta_2) &= G(|\vec{\alpha}|, \beta_1) G(|\vec{\alpha}|, \beta_2), \\ G(|\vec{\alpha}_1 + \vec{\alpha}_2|, \beta) &= G(|\vec{\alpha}_1|, \beta) G(|\vec{\alpha}_2|, \beta) e^{i\beta \vec{\alpha}_1 \cdot \vec{\alpha}_2}, \\ \int d\vec{\alpha} G(|\vec{\alpha}|, \beta) e^{i\vec{\gamma} \cdot \vec{\alpha}} &= i \frac{2\pi}{\beta} G(|\vec{\gamma}|, -\frac{1}{\beta}). \end{aligned} \quad (A-7)$$

Notice that the last equation in Eq. (A-7) is the Fourier transform of the $G(|\vec{\alpha}|, \beta)$ function. As we shall see in the following, these properties are very useful in simplifying the calculations of the Green's functions $g(\vec{\kappa}, \omega; \vec{\rho}, z)$.

Next, we consider inserting an imaginary plane σ' between σ_0 and σ . This is equivalent to having two consecutive Fresnel propagations with a diffraction-free σ' plane of infinity. Thus, the calculation of these consecutive Fresnel propagations should yield the same Green's function as that of the above direct Fresnel propagation shown in Eq. (A-6):

$$\begin{aligned} &g(\omega, \vec{\kappa}; \vec{\rho}, z) \\ &= C^2 \frac{e^{i\frac{\omega}{c}(d_1+d_2)}}{d_1 d_2} \int_{\sigma'} d\vec{\rho}' \int_{\sigma_0} d\vec{\rho}_0 \tilde{A}(\vec{\rho}_0) G(|\vec{\rho}' - \vec{\rho}_0|, \frac{\omega}{cd_1}) G(|\vec{\rho} - \vec{\rho}'|, \frac{\omega}{cd_2}) \\ &= C \frac{e^{i\frac{\omega}{c}z}}{z} \int_{\sigma_0} d\vec{\rho}_0 \tilde{A}(\vec{\rho}_0) G(|\vec{\rho} - \vec{\rho}_0|, \frac{\omega}{cz}) \end{aligned} \quad (A-8)$$

where C is a necessary normalization constant for a valid Eq. (A-8), and $z = d_1 + d_2$. The double integral of $d\vec{\rho}_0$ and $d\vec{\rho}'$ in Eq. (A-8) can be evaluated as

$$\begin{aligned}
& \int_{\sigma'} d\vec{\rho}' \int_{\sigma_0} d\vec{\rho}_0 \tilde{A}(\vec{\rho}_0) G(|\vec{\rho}' - \vec{\rho}_0|, \frac{\omega}{cd_1}) G(|\vec{\rho} - \vec{\rho}'|, \frac{\omega}{cd_2}) \\
&= \int_{\sigma_0} d\vec{\rho}_0 \tilde{A}(\vec{\rho}_0) G(\vec{\rho}_0, \frac{\omega}{cd_1}) G(\vec{\rho}, \frac{\omega}{cd_2}) \\
&\quad \times \int_{\sigma'} d\vec{\rho}' G(\vec{\rho}', \frac{\omega}{c}(\frac{1}{d_1} + \frac{1}{d_2})) e^{-i\frac{\omega}{c}(\frac{\vec{\rho}_0}{d_1} + \frac{\vec{\rho}}{d_2}) \cdot \vec{\rho}'} \\
&= \frac{i2\pi c}{\omega} \frac{d_1 d_2}{d_1 + d_2} \int_{\sigma_0} d\vec{\rho}_0 \tilde{A}(\vec{\rho}_0) G(\vec{\rho}_0, \frac{\omega}{cd_1}) G(\vec{\rho}, \frac{\omega}{cd_2}) \\
&\quad \times G(|\frac{\vec{\rho}_0}{d_1} + \frac{\vec{\rho}}{d_2}|, \frac{\omega}{c}(\frac{d_1 d_2}{d_1 + d_2})) \\
&= \frac{i2\pi c}{\omega} \frac{d_1 d_2}{d_1 + d_2} \int_{\sigma_0} d\vec{\rho}_0 \tilde{A}(\vec{\rho}_0) G(|\vec{\rho} - \vec{\rho}_0|, \frac{\omega}{c(d_1 + d_2)})
\end{aligned}$$

where we have applied Eq. (A-7), and the integral of $d\vec{\rho}'$ has been taken to infinity. Substituting this result into Eq. (A-8) we obtain

$$\begin{aligned}
& g(\vec{\kappa}, \omega; \vec{\rho}, z) \\
&= C^2 \frac{i2\pi c}{\omega} \frac{e^{i\frac{\omega}{c}(d_1 + d_2)}}{d_1 + d_2} \int_{\sigma_0} d\vec{\rho}_0 \tilde{A}(\vec{\rho}_0) G(|\vec{\rho} - \vec{\rho}_0|, \frac{\omega}{c(d_1 + d_2)}) \\
&= C \frac{e^{i\frac{\omega}{c}z}}{z} \int_{\sigma_0} d\vec{\rho}_0 \tilde{A}(\vec{\rho}_0) G(|\vec{\rho} - \vec{\rho}_0|, \frac{\omega}{cz}).
\end{aligned}$$

Therefore, the normalization constant C must take the value of $C = -i\omega/2\pi c$. The normalized Green's function for free-space Fresnel propagation is thus

$$g(\vec{\kappa}, \omega; \vec{\rho}, z) = \frac{-i\omega}{2\pi c} \frac{e^{i\frac{\omega}{c}z}}{z} \int_{\sigma_0} d\vec{\rho}_0 \tilde{A}(\vec{\rho}_0) G(|\vec{\rho} - \vec{\rho}_0|, \frac{\omega}{cz}). \quad (A-9)$$

References

- [1] T.B. Pittman, Y.H. Shih, D.V. Strekalov, and A.V. Sergienko, Phys. Rev. A **52**, R3429 (1995).
- [2] D.N. Klyshko, Usp. Fiz. Nauk, **154**, 133 (1988); Sov. Phys. Usp, **31**, 74 (1988); Phys. Lett. A **132**, 299 (1988).
- [3] D.V. Strekalov, A.V. Sergienko, D.N. Klyshko and Y.H. Shih, Phys. Rev. Lett. **74**, 3600 (1995).
- [4] A. Einstein, B. Podolsky, and N. Rosen, Phys. Rev. **35**, 777 (1935).
- [5] G. Scarcelli, V. Berardi, and Y.H. Shih, Phys. Rev. Lett. **96**, 063602 (2006).
- [6] A. Valencia, G. Scarcelli, M. D'Angelo, and Y.H. Shih, Phys. Rev. Lett. **94**, 063601 (2005).
- [7] G. Scarcelli, A. Valencia, and Y.H. Shih, Europhys. Lett. **68**, 618 (2004).
- [8] R. Meyers, K.S. Deacon, and Y.H. Shih, Phys. Rev. A **77**, 041801(2008).

- [9] Y.H. Shih, IEEE J. of Selected Topics in Quantum Electronics, **9**, 1455 (2003).
- [10] R.S. Bennink, S.J. Bentley, and R.W. Boyd, Phys. Rev. Lett. **89**, 113601 (2002); R.S. Bennink, *et al.*, Phys. Rev. Lett. **92**, 033601 (2004).
- [11] A. Gatti, E. Brambilla, M. Bache and L.A. Lugiato, Phys. Rev. A **70**, 013802, (2004), and Phys. Rev. Lett. **93**, 093602 (2004)
- [12] K. Wang, D. Cao, quant-ph/0404078; D. Cao, J. Xiong, and K. Wang, quant-ph/0407065.
- [13] Y.J. Cai, and S.Y. Zhu, quant-ph/0407240, Phys. Rev. E, **71**, 056607 (2005).
- [14] B.I. Erkmen and J.H. Shapiro, Phys. Rev. A **77**, 043809 (2008).
- [15] R. Hanbury-Brown, and R.Q. Twiss, Nature, **177**, 27 (1956); **178**, 1046, (1956); **178**, 1447 (1956).
- [16] R. Hanbury-Brown, *Intensity Interferometer*, Taylor and Francis Ltd, London, 1974.
- [17] M.O. Scully and M.S. Zubairy, *Quantum Optics*, Cambridge University Press, Cambridge, 1997.
- [18] M. H. Rubin, Phys. Rev. A **54**, 5349 (1996).
- [19] J. W. Goodman, *Introduction to Fourier Optics*, McGraw-Hill Publishing Company, New York, NY, 1968.
- [20] D.N. Klyshko, *Photon and Nonlinear Optics*, Gordon and Breach Science, New York, 1988.
- [21] M. D'Angelo, A. Valencia, M.H. Rubin, and Y.H. Shih, Phys. Rev. A **72**, 013810 (2005).
- [22] J.C. Howell *et al.*, Phys. Rev. Lett., **92**, 210403 (2004).
- [23] W. Martienssen and E. Spiller, Am. J. Phys. **32**, 919 (1964).
- [24] R.J. Glauber, Phys. Rev. **130**, 2529 (1963); Phys. Rev. **131**, 2766 (1963).
- [25] A. Gatti *et al.*, Phys. Rev. Lett. **98**, 039301 (2007) (comment); G. Scarcelli, V. Berardi, and Y.H. Shih, Phys. Rev. Lett. **98**, 039302 (2007) (reply).
- [26] F. Ferri, *et al.*, Phys. Rev. Lett. **94**, 183602 (2005).
- [27] J.B. Liu, Y. Zhou, G.Q. Zhang, and Y.H. Shih (to be published).